TiO$_2$ Photocatalytic Degradation of Waste Activated Sludge and Potassium Hydrogen Phthalate in Wastewater for Enhancing Biogas Production

May 2013

Dawei LI

TiO$_2$ Photocatalytic Degradation of Waste Activated Sludge and Potassium Hydrogen Phthalate in Wastewater for Enhancing Biogas Production

A Dissertation Submitted to

the Graduate School of Life and Environmental Sciences,

the University of Tsukuba

in Partial Fulfillment of the Requirements

for the Degree of Doctor of Philosophy in Environmental Studies

(Doctoral Program in Sustainable Environmental Studies)

Dawei LI

Abstract

Worldwide, increasing amounts of waste activated sludge (WAS) pose a great challenge to the local wastewater treatment plant. Anaerobic digestion of WAS is of considerable interest due to its bioenergy recovery, value-added products manufacture and greenhouse gas emission control. However, the hydrolysis rate of insoluble macromolecular components, such as polysaccharides, proteins, and lipids, limits the overall biodegradation rate of WAS. On the other hand, the contamination of water caused by recalcitrant organic pollutants, like organic dyes, pesticides and antibiotics, affects seriously the quality of water source. The release of these persistent organics into natural environment is not only hazardous to aquatic life but also in many cases mutagenic to humans and animals. The treatment of wastewater containing such compounds is very important for the protection of water source and environment.

Heterogeneous photocatalytic oxidation is a promising alternative among advanced oxidation processes (AOPs), due to easy operation under ambient temperature and pressure. In addition, TiO_2 has been proven to be the most suitable photocatalyst because of its high chemical stability, strong photocatalytic activity, inexpensive and nontoxicity. TiO_2 photocatalysis seems to be a potential option to enhance the hydrolysis of macromolecular components of WAS and degradation of recalcitrant organic pollutants in wastewater. The aim of this study is to investigate the effects of TiO_2 photocatalytic pretreatment on the biodegradability of WAS and develop a high-efficiency immobilized photocatalytic reactor for the decomposition

of recalcitrant organics (Rhodamine B, Methyl Orange, and Potassium Hydrogen Phthalate) in wastewater.

Firstly, the effects of TiO_2 photocatalysis on the hydrolysis of protein of waste activated sludge and its biodegradability were investigated. The photocatalytic degradation of protein was carried out by a slurry suspension system at $25^{o}C$, using bovine serum albumin (500 mg L^{-1}) as the protein model and nano-sized TiO_2 particles (anatase, 20 nm) as the photocatalyst. After 12-h UV irradiation, the percentage degradation of protein by TiO_2 photocatalytic oxidation reached 98.1%. The optimal condition for photocatalytic degradation of protein is TiO_2 dosage of 5.0 mg L^{-1} under 2.4 w m^{-2} UV light irradiation. The same TiO_2 photocatalytic system was employed as experimental apparatus in the pretreatment of waste activated sludge, and the photocatalysis pretreated WAS was used as substrate in the following mesophilic biohydrogen fermentation. After 96-h mesophilic fermentation, the hydrogen production from TiO_2 photocatalysis pretreated WAS reached 11.7 mL-H_2/g-VS, which was 2.2 times of that from the control. TiO_2 photocatalytic pretreatment of WAS obviously accelerated the hydrolysis of its macromolecular components like protein and improved the hydrogen production in the subsequent mesophilic fermentation.

After that, a novel TiO_2-coated beads immobilized photocatalytic reactor (TBIPR) was developed and successfully applied for the decomposition of recalcitrant organics in wastewater using Rhodamine B (RhB) and Methyl Orange (MO) as the model compounds. The TBIPR was developed by immobilizing 84.0 g

TiO$_2$-coated silica beads (average diameter: 3 mm) in a cylindrical-shell photoreactor which axially inserted with an UV black light lamp (power: 10 w, λ_{max}: 365 nm). The average UV intensity in the developed TBIPR is 10 w m^{-2} and its working volume is 800 mL. The prepared 1200 mL of each dye solution (10 mg L^{-1}) was separately induced into the photocatalytic reactor and continuously circulated by a peristaltic pump. The photocatalytic degradation of each dye was conducted at 25°C under 10 w m^{-2} UV irradiation. The operation parameters including flow rate, initial concentration and repetitive operation performance were investigated. The optimal flow rate is 50 mL min^{-1} in this study. The increase of initial RhB concentration leads to the decrease of photocatalytic degradation. Five repetitive operations gave a relative standard deviation of 0.32%, indicating that the photocatalytic performance of developed TBIPR remains almost constant. The results demonstrated that the developed TBIPR is a promising alternative for decomposing recalcitrant organics like RhB and MO in wastewater.

Then, the developed TBIPR was used for the treatment of high-COD wastewater synthesized using potassium hydrogen phthalate (KHP) as target organic pollutant, and the TiO$_2$ photocatalysis pretreated KHP wastewater was used for methane fermentation. The photocatalytic degradation of KHP (5000 mg L^{-1}) was performed using the developed photocatalytic reactor with the flow rate of 50 mL min^{-1}. The COD removal by 30-d photocatalytic treatment using developed TBIPR reached 57.26%. Then, after 14-d mesophilic anaerobic fermentation, the methane production from TiO$_2$ photocatalysis pretreated KHP wastewater reached 146.70

mL-CH$_4$/g-COD, which was much higher than that of the control (6.99 mL-CH$_4$/g-COD). The developed TBIPR exhibited excellent performance for the treatment of synthesized high-COD wastewater containing non-biodegradable KHP, and facilitated the methane production in its following anaerobic fermentation.

Contents

Figures

Tables

Chapter 1 Introduction

1.1 Background

In past decades, increasing amounts of municipal, industrial and domestic wastewaters were generated worldwide with the continuous development of modern industry and world population. Activated sludge process is a most widely used technique for biological wastewater treatment in the world, due to its easy operation, high treatment efficiency and low operation cost. However, it results in a huge production of waste activated sludge (WAS) in wastewater treatment plants (WWTPs). The treatment and disposal of WAS generally accounts for 50%-60% of the total construction and operation costs of a WWTP [1], which in addition to the serious environmental impacts of WAS poses a great challenge to local WWTPs.

Three main alternatives are usually considered for WAS disposal including landfilling, incineration, and fertilizer utilization. Nevertheless, they all cause various socioeconomic-ecological problems limiting or even hindering their applications. Landfilling is one of the common ways to deal with wastes, but it is not sustainable since its secondary pollution like odor emission and the limited land space. Incineration of wastes is usually expensive and emits volatiles/toxicants which prone to cause atmospheric pollution. The utilization of WAS as agricultural fertilizer is strictly regulated due to both potentially toxic compositions, such as heavy metals, pathogens and persistent organic pollutants, and unworthy long-distance transportation to faraway countryside [2]. Therefore, it is necessary to develop cost-efficient and environmental friendly alternatives for the management of

generated large quantities of WAS.

On the other hand, the contamination of water caused by recalcitrant organic pollutants, such as organic dyes, pesticides and antibiotics, affects seriously the quality of water resource. The release of these recalcitrant organics into natural environment is not only hazardous to aquatic life but also in many cases mutagenic to humans and animals. The treatment of wastewaters containing such compounds is very important for the protection of water sources and environment. Conventional physicochemical methods including adsorption, filtration, and flocculation merely transfer the organic contaminants from one phase to another phase which requiring a further treatment [3]. The biological method has been proven to be inefficient in decontaminating the wastewater containing recalcitrant organics [4]. Thus, alternative advanced techniques are required for the decomposition of recalcitrant organic contaminants in wastewater.

1.2 Anaerobic digestion of waste activated sludge

Anaerobic digestion of waste activated sludge is a promising alternative to landfilling, incineration, and fertilizer utilization, mainly due to energy recovery by biogas collection and a reduction in CO_2 emission. In addition, it has the ability to reduce approximately 40% volume of the wastes by degrading its organic components into biogas (55%-70% CH_4) and disinfect pathogenic microorganisms. Actually, WAS is rich in organic carbon, so it can be used as a valuable resource for bioenergy conversion rather than be discharged as a waste. Thus, anaerobic digestion is an economic and environmental friendly technology for the management of

generated huge amounts of WAS.

1.2.1 Theory of anaerobic digestion

Anaerobic digestion is a multi-step biochemical reaction process in which organic matters are mineralized to methane and carbon dioxide by diverse microorganisms. Generally, the anaerobic digestion process consists the following four steps: hydrolysis, acidogenesis, acetogenesis, and methanogenesis [5]. Various microorganisms are involved in each step. The anaerobic digestion process of organic substrates was illustrated in Fig. 1.1.

During the first step, a group of hydrolytic bacteria secretes enzymes that hydrolyze macromolecular polymers to micromolecular monomers to converts the insoluble substrates to soluble compounds [6]. The hydrolytic bacteria remove the small amounts of oxygen present and create an anaerobic condition in the bioreactor. Subsequently, diverse group of acidogenic bacteria ferment the hydrolysate to produce organic acids, H_2 and CO_2. In the subsequent step, acetogenic bacteria convert the soluble monomers to acetic acids. The final step in biogas production is performed by acetoclastic/hydrogenotrophic methanogens, which produce methane from either acetate or H_2 and CO_2 [7].

1.2.2 Rate-limiting step of anaerobic digestion process

In a sound anaerobic digestion system, the four biological processes occur sequentially and simultaneously. Hydrolysis of insoluble polymers to soluble hydrolysate is usually considered as a rate-limiting step of overall anaerobic

digestion process especially when the substrate is in particulate form [8]. The hydrolytic process includes multiple enzyme production, diffusion, adsorption, reaction and deactivation steps [9], which coupling with hydrolysate formation, liberation, dispersion, utilization and accumulation [10]. Hydrolysis is dependent on the substrate accessibility and enzyme availability, which is the most vulnerable step to pH and the accumulation of short-chain organic acids that affect the stability of the whole process.

1.2.3 Pretreatment of waste activated sludge

Bioconversion of WAS to biogas is intermediated by hydrolytic and acidogenic processes. The hydrolysis of macromolecular components depends heavily on hydrolytic enzymes and limits the biodegradation rate of WAS. Thus, suitable pretreatment prior to anaerobic digestion is required for enhancing the biodegradability of WAS.

Many pretreatments involving mechanical [11], thermal [12], acid [13], alkaline [14], ultrasonication [15] and advanced oxidation process (AOPs) [16, 17] have been implemented successfully to enhance the hydrolysis of macromolecular components of WAS. Among these methods, AOPs exhibit great potentiality for enhancing the hydrolysis of macromolecular components in WAS since its generation of highly reactive hydroxyl radicals (OH) that could oxidize various organics quickly and non-selectively [18]. Nevertheless, taking the energy saving and environmental conservation into account, development of more cost-efficient and environmental friendly pretreatment of WAS is necessary.

4

1.3 Photocatalytic degradation of waste activated sludge and recalcitrant organic contaminants in wastewater

Photocatalytic oxidation is a promising alternative among AOPs. Generally, photocatalytic oxidation can be defined as an acceleration of photoinduced reaction by the presence of photocatalyst [19]. Such photocatalysts in a heterogeneous photocatalysis are solid semiconductor materials, such as titanium dioxide (TiO_2), tungsten trioxide (WO_3), zinc oxide (ZnO) and vanadium pentoxide (V_2O_5). Amongst them, TiO_2 has been proven to be the most suitable photocatalyst because of its high chemical stability, strong photocatalytic activity, inexpensive and nontoxicity [20]. Since the easy operation under ambient temperature and pressure, TiO_2 photocatalytic oxidation seems to be a potential alternative for the pretreatment of WAS and decomposition of recalcitrant organic contaminants in wastewater.

1.3.1 Mechanism of heterogeneous photocatalytic oxidation

Photoinduced reactions are activated by absorption of a photon (hυ) with sufficient energy that equals or exceeds the band gap energy (E_g) of the photocatalyst [19]. The mechanism of TiO_2 photocatalytic oxidation of organic compounds under UV light irradiation can be described as follows:

$$TiO_2 + h\upsilon \rightarrow TiO_2(e^-_{cb} + h^+_{vb}) \qquad (1\text{-}1)$$

$$TiO_2(h^+_{vb}) + H_2O \rightarrow TiO_2 + H^+ + \cdot OH \qquad (1\text{-}2)$$

$$TiO_2(h^+_{vb}) + OH^- \rightarrow TiO_2 + \cdot OH \qquad (1\text{-}3)$$

$$TiO_2(e^-_{cb}) + O_2 \rightarrow TiO_2 + O_2^- \cdot \qquad (1\text{-}4)$$

$$Organics + \cdot OH \rightarrow Degradation\ products \qquad (1\text{-}5)$$

5

$$Organics + TiO_2(h^+_{vb}) \rightarrow Oxidation\ products \qquad (1\text{-}6)$$

$$Organics + TiO_2(e^-_{cb}) \rightarrow Reduction\ products \qquad (1\text{-}7)$$
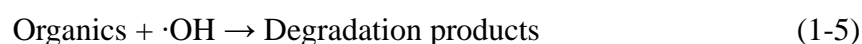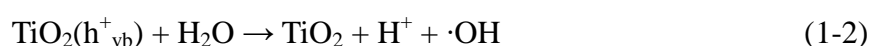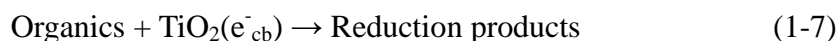
When the photocatalyst absorbs a photon of energy equals or higher than its band gap width ($h\upsilon \geq E_g$), an electron (e^-) may be excited from the valence band (VB) to the conduction band (CB), resulting in generation of an electron-hole pair (e^-_{cb}-h^+_{vb}) (Eq. (1-1), Fig. 1.2). Then the electron and hole migrates to the catalyst surface and recombines quickly unless reacting with the surface-adsorbed substances. The highly oxidative holes can react with surface-bond water molecules or hydroxyl ions to produce ·OH radicals (Eqs. (1-2) and (1-3)), whereas the excited electrons can be scavenged by oxygen to form superoxide radical anions ($O_2^-·$) (Eq. (1-4)). The highly reactive species (·OH, h^+_{vb}, and $O_2^-·$) possess the potential to decompose various organics via a series of redox reactions (Eqs. (1-5)-(1-7)). Eventually, the degradation products involving CO_2, water, nitrates and sulfates are generated after the heterogeneous photocatalytic oxidation of target organics.

1.3.2 Factors affecting the photocatalytic efficiency

The efficiency of a photocatalytic oxidation process is affected by many operating parameters, such as configuration of the photocatalytic reactor, loading of the photocatalyst, initial concentration and pH of the reactant, light intensity and the presence of ions. For a high-efficiency heterogeneous photocatalytic oxidation process, it is very important to optimize these operation parameters.

(1) Configuration of the photocatalytic reactor

In general, the photocatalytic reactors can be divided into two main types:

slurry-suspension photoreactors and catalyst-immobilization photoreactors. Each configuration has its advantages and disadvantages. The photocatalytic efficiency of slurry-suspension photoreactors is generally higher than that of catalyst-immobilization photoreactors, due to the high surface area for adsorption and reaction. However, its low light utilization efficiency and difficult separation/recovery of nano-particulate photocatalysts after the reaction constrains the application of this design. Development of membrane photocatalytic reactor (MPR) which coupled the pressure-driven membrane filtration with slurry type photoreactor has shown to solve the issue of photocatalysts separation [21]. Nevertheless, this process needs pressure, and fouling of the membrane limits the synergy of such combination [22, 23]. To overcome the deficiency of slurry-suspension photoreactors, the immobilization of photocatalysts on a carrier material or within the photoreactor has also attracted increasing concern in recent years. Whereas, this type photoreactors are usually characterized by a low surface-to-volume ratios and inefficiencies introduced by absorption and scattering of photons by the lighttight support materials and the reaction medium [24]. For enhancing the photocatalytic efficiency of catalyst-immobilization photoreactors, it is essential to synthesize a high-translucency photocatalyst possessing high adsorption capacity and/or modify the configuration of photocatalytic reactor.

(2) Loading of the photocatalyst

The loading of photocatalyst is one of the most important factors that influence the photocatalytic efficiency. Increasing the photocatalyst loading can increase the

available surface area for adsorption and reaction. However, increasing of the photocatalyst concentration also increases the solution opacity leading to a decrease of light penetration intensity in the photoreactor [25]. Moreover, the agglomeration of photocatalyst nanoparticles at high solid concentration results in the loss of the surface area [26]. To some extent, the initial rates of photocatalytic reaction are directly proportional to the mass of photocatalysts present in the solution. Nevertheless, when the loading of photocatalyst exceeds a certain level, the photocatalytic reaction rate becomes independent of photocatalyst concentration. Thus, to select an optimum loading of photocatalyst is required for ensuring a high efficiency of the photocatalytic reaction system.

(3) pH and initial concentration of the reactant

The effects of pH on photocatalytic degradation of target organics in aqueous solution mainly associated with the ionization state of photocatalyst surface, position of the valence and conduction bands of the photocatalyst, agglomeration of photocatalyst nanoparticles and the formation of hydroxyl radicals [27]. Taking TiO_2 as an example, the isoelectric point (point of zero charge, pzc) of the most commonly used TiO_2 Degussa P25 is at pH 6.8. The TiO_2 surface is positively charged in acidic media (pH < 6.8), while it is negatively charged under alkaline conditions (pH > 6.8) [27]. What means that at pH > pzc the photocatalysts mainly adsorb positively charged contaminants, whereas at pH < pzc the adsorption of negatively charged contaminants is favored. TiO_2 nanoparticles prone to agglomerate under acidic conditions, and the surface area available for adsorption of

contaminants and photon absorption would be reduced that finally affects the photocatalytic degradation efficiency [28]. In alkaline conditions, the ·OH radicals are easier generated since more OH^- ions are available on TiO_2 surface, resulting in an improvement of the photocatalytic efficiency. In contrast, at low pH level the positive holes are considered as the major oxidative species. Since the effect of pH is so complicated, an optimal pH level should be selected for a specified application on a basis of preliminary experiments.

The initial concentration influences the photocatalytic efficiency mainly via affecting the light penetration intensity and the ratio of photoproduced reactive radicals to organic molecules in the reaction system. The photocatalytic degradation rate of target organics increases with increasing initial concentration to a certain level, then further increasing the initial concentration leads to a decrease of the degradation rate [27].

(4) Light intensity

The effects of light intensity on the photocatalytic efficiency can be described as follows [29]: (a) At low light intensity (0-200 w m^{-2}), the reaction rate increases linearly with increasing light intensity, since the predominant reaction is electron-hole formation rather than electron-hole recombination. (b) At intermediate light intensity (approximately 250 w m^{-2}), the reaction rate depends on the square root of the light intensity, because electron-hole pair separation competes with recombination, thereby resulting in lower effect on the reaction rate. (c) At high light intensity, the reaction rate is independent of light intensity. The generation of $O_2^-·$

radicals is the rate-limiting step especially in case of larger TiO_2 particles and the photocatalysts agglomerate [30].

(5) The presence of ions

Many inorganic anions naturally existing in waters, such as Cl^-, NO_3^-, SO_4^{2-}, CO_3^{2-} and HCO_3^-, usually act as the scavengers of h^+_{vb} and $\cdot OH$ in the reaction system [27]. Then, some inorganic anion radicals like $NO_3\cdot$ and $CO_3\cdot$ that exhibit lower reactivity than h^+_{vb} and $\cdot OH$ are generated. The observed decrease of photocatalytic efficiency in the presence of inorganic ions mainly due to the adsorption of these anions on TiO_2 surface [31].

1.3.3 Challenges of TiO_2 photocatalytic degradation of waste activated sludge and recalcitrant organic contaminants in wastewater

The major obstacle in TiO_2 photocatalytic degradation of WAS is the inhibited UV light transmission caused by its deep color and high-concentration suspension solid characteristics. Enhancing the translucency of WAS to ensure sufficient photons transmission in the reaction system is essential for an efficient photocatalytic degradation of WAS. On the other hand, currently used photocatalytic reactor for liquid phase oxidation is based mainly on the slurry-suspension type. In order to achieve an easy separation/recovery of the TiO_2 photocatalyst after the reaction, the immobilization of photocatalysts on a support material or within the photoreactor is desirable. In addition, there is great need to enhance the light utilization efficiency in the photocatalytic reaction system by modifying the configuration of photocatalytic reactor.

1.4 Objectives of this thesis

The introduction part has concluded that TiO_2 photocatalysis is a potential option to enhance the hydrolysis of macromolecular components of WAS. The aim of this study is to investigate the effects of TiO_2 photocatalytic pretreatment on the biodegradability of WAS and develop a high-efficiency immobilized photocatalytic reactor for the decomposition of recalcitrant organics in wastewater. The specific objectives are listed as follows:

(1) Investigate the effects of TiO_2 photocatalysis on the nonenzymatic hydrolysis of specific macromolecular components of WAS using bovine serum albumin as a protein model.

(2) Evaluate the potential of TiO_2 photocatalytic pretreatment for enhancing the biodegradability and biohydrogen producibility of WAS.

(3) Develop a novel immobilized photocatalytic reactor using TiO_2-coated beads and evaluate its photocatalytic efficiency by monitoring the photocatalytic degradation of Rhodamine B and Methyl Orange in aqueous solution.

(4) Investigate the photocatalytic performance of developed photocatalytic reactor to treat high-COD loading wastewater synthesized by potassium hydrogen phthalate (KHP), and use the photocatalytic pretreated KHP wastewater for methane fermentation.
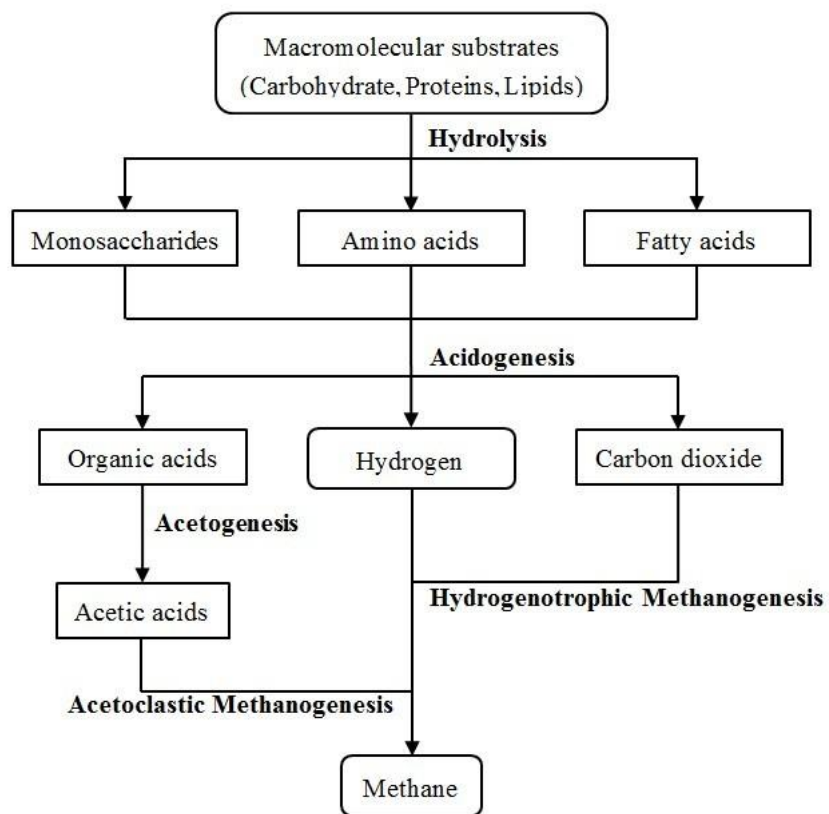
Fig 1.1 Anaerobic digestion process of organic substrate.
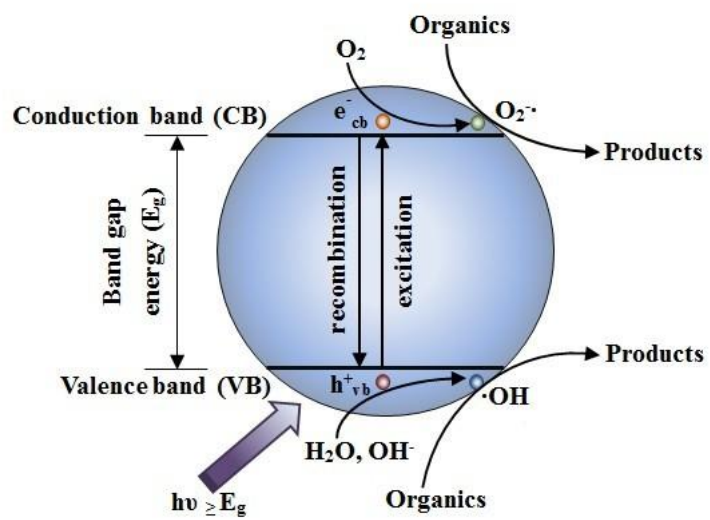
Fig 1.2 Mechanism of heterogeneous photocatalytic oxidation.

Chapter 2 Using TiO$_2$ photocatalysis as a pretreatment of waste activated

sludge to enhance the biohydrogen production

2.1 Introduction

Worldwide, increasing amounts of waste activated sludge (WAS) pose a great challenge to local wastewater treatment plants due to its environmental impacts, as well as huge treatment and disposal costs. The treating and disposing costs of WAS account for 60% operation cost of wastewater treatment plant [32]. WAS is rich in organic carbon, and so it can be used as a valuable resource for bioenergy conversion rather than be discharged as a waste. Anaerobic digestion of WAS is of considerable interest owing to its bioenergy recovery in the form of biogas (H$_2$/CH$_4$) [33, 34], value-added products manufacture like organic acids [35] and reduction of greenhouse gas emission [36]. Bioconversion of organic carbon-rich WAS to biogas is intermediated by hydrolytic and acidogenic processes. The hydrolysis of macromolecular components (proteins, polysaccharides and lipids) depends heavily on hydrolytic enzymes, e.g., proteases, glucosidases and lipases, and limits the biodegradation rate of WAS. Thus, suitable pretreatment prior to anaerobic digestion is desirable for enhancing the biodegradability of WAS.

In recent years, many pretreatments have been proposed and shown to facilitate the hydrolysis of macromolecular components of WAS. These pretreatments involve mechanical disintegration [37], thermal hydrolysis [38, 39], acid [40]/alkaline [41] solubilization, ultrasonication [42, 43], and advanced oxidation processes (AOPs)

using Ozone [44], hydrogen peroxide [45] and peracetic acid [46]. Amongst them, AOPs using strong oxidizing agents exhibit significant potential to accelerate the hydrolysis of macromolecular components as the generation of highly reactive hydroxyl radicals (OH). However, from the viewpoint of energy saving and environmental conservation, developing a more cost-efficient and environmental friendly pretreatment is essential.

Heterogeneous photocatalytic oxidation using TiO_2 is a promising alternative among AOPs for decomposing environmental contaminants, since the easy operation under ambient temperature and pressure and the possibility of using solar light as irradiation source. In addition, TiO_2 has been proven to be the most suitable photocatalyst because of its high chemical stability, strong photocatalytic activity, inexpensive and nontoxicity [47]. Although the reaction mechanism of AOPs in general is the generation of highly reactive OH, the photocatalytic degradation of organics over TiO_2 particles occurs mainly via the formation of holes (h_{vb}^+) [48]. When the absorbed photon energy equals or exceeds the band gap of semiconductor photocatalyst, electrons are excited from the valence band (VB) to the conduction band (CB), resulting in formation of a high energy electron-hole pair (e_{cb}^--h_{vb}^+). The photoproduced electron-hole pairs migrate to the photocatalyst surface and recombine quickly unless reacting with the surface-sorbed substances. The excited electrons are scavenged by oxygen to form superoxides ($O_2^{\cdot -}$) and the highly oxidative holes react with either water molecules or hydroxyl ions to yield OH radicals [49]. The oxidizing species (h_{vb}^+, OH, and $O_2^{\cdot -}$) possess the potential to

15

oxidize various organics. TiO$_2$ photocatalysis has been widely used to decompose some recalcitrant contaminants such as methyl orange [50], rhodamine B [51], malachite green [52], and humic acids [53] in wastewater. In the biomedical field, TiO$_2$ photocatalysis exhibits a great potential for surface decontamination of medical devices and implants by changing the conformation of proteins and accelerating its nonenzymatic degradation [54]. TiO$_2$ photocatalysis seems to be a promising pretreatment of WAS for enhancing its biodegradability by accelerating the hydrolysis of specific macromolecular components such as proteins. However, there is few report on using TiO$_2$ photocatalysis as a pretreatment of WAS to accelerate the hydrolysis of its macromolecular components.

In this study, TiO$_2$ photocatalysis was used as a pretreatment of waste activated sludge to enhance its biodegradability. The objective of this work was to investigate the effects of TiO$_2$ photocatalysis on the nonenzymatic hydrolysis of specific macromolecular components of WAS using bovine serum albumin as a protein model; and evaluate the potential of TiO$_2$ photocatalytic pretreatment for enhancing the biodegradability and biohydrogen producibility of waste activated sludge.

2.2 Materials and methods

2.2.1 Materials

Bovine serum albumin (BSA) obtained from Wako Pure Chemical Industries, Ltd. (Osaka, Japan) was simulated as the proteins of WAS. Before the experiments, protein solution containing 500 mg L^{-1} of BSA in 0.15 mol L^{-1} NaCl buffer solution

was prepared and stored at 4 ^{o}C in a fridge. The waste activated sludge (WAS) sample was taken from the secondary sedimentation tank of a wastewater treatment plant located in Shimodate (Ibaraki, Japan). Prior to use, the collected WAS was stored in a refrigerator at 4°C. Its characteristics were analyzed before the experiments and are listed in Table 3.1. The TiO$_2$ photocatalyst (STS-21, 20 nm) was provided by Ishihara Sangyo Kaisha, LTD. Properties of the photocatalyst are as follows: TiO$_2$ content (39.2 %, 1000 mg/L), pH (8.3), Absorbance (0.43), Viscosity (42.2).

2.2.2 TiO$_2$ photocatalytic hydrolysis of simulated proteins of WAS

To investigate the effect of TiO$_2$ photocatalytic oxidation on the hydrolysis of macromolecular components of WAS, a series of batch experiments were carried out using bovine serum albumin (BSA) as a protein model. A conventional suspension system was used as the experimental apparatus, which consists of a 300 mL glass beaker (diameter: 90 mm, height: 60 mm) with cover, an UV black light lamp (length: 300 mm; diameter: 28 mm; power: 10 w) as the irradiation source, and a magnetic stirrer (SRS116AA, ADVANTEC, Japan).

The photocatalytic degradation of proteins were carried out by adding 120 mL BSA solution and TiO$_2$ photocatalyst in the reactor at the desired concentration (5 mg L^{-1}). Before irradiation, the suspension was magnetically stirred for 30 min in the dark to achieve an adsorption/desorption equilibrium. Then the UV lamp was switched on to initiate the photocatalytic reaction. During irradiation, samples (1 mL) were taken and centrifuged (12,000 $\times$g, 10 min) at every 1 h up to 12 h. The protein

concentration was measured with a UV-vis spectrophotometer (UV1800, SHIMADZU, Japan) at 595 nm using coomassie brilliant blue method. Duplicate experiments were conducted under the same condition, and the mean values were used for analyses.

In order to optimize the operation parameters in this study, the photocatalytic degradation of proteins (500 mg L^{-1}) at different TiO_2 dosage (0, 2.5, 5.0, 7.5 and 10.0 mg L^{-1}) were conducted. The effect of UV light intensity on the photocatalytic degradation of proteins with the TiO_2 dosage of 5.0 mg L^{-1} was carried out in the range of 0-5 w m^{-2}. The sampling and measurement methods are the same as previous described.

2.2.3 TiO_2 photocatalytic pretreatment of WAS

Given the deep color and high-concentration suspension solid characteristics of raw WAS, that may inhibit UV light transmission in the photocatalytic pretreatment of WAS, it was diluted to 10-fold using deionized water before pretreatment. The characteristics of diluted WAS were shown in Table 3.1. The same suspension system was used as the experimental apparatus for TiO_2 photocatalytic pretreatment of WAS.

The photocatalytic pretreatment of WAS were performed by adding 120 mL diluted WAS (dilution ratio: 0, 5, 10, and 15-fold) and TiO_2 photocatalyst in the reactor at the desired concentration (5 mg L^{-1}). Before irradiation, the suspension was magnetically stirred for 30 min in the dark to achieve the equilibrium. Then the UV light irradiation with intensity of 5.0 w m^{-2} was conducted to initiate the

photocatalytic reaction. During experiments, samples (1 mL) were taken at a time interval of 1 h up to 12 h. The general characteristics such as total solid content (TS), volatile solid content (VS), chemical oxygen demand (COD) and ammonium concentration (NH_4^+-N) of TiO_2 photocatalysis pretreated WAS were determined according to the standard methods. Duplicate experiments were carried out under the same condition, and the mean values were used for analyses.

2.2.4 Fermentative biohydrogen production from TiO_2 photocatalysis pretreated WAS

In order to accelerate the start-up process and achieve a stable hydrogen fermentation system, pretreatment of the seed sludge is required to enrich hydrogen-producing bacteria. Acidification, in comparison with other methods, is a simple, economic and effective pretreatment for enriching hydrogen-producing bacteria from WAS [55]. In this study, an acidification pretreatment of raw WAS was conducted to enrich the hydrogen-producing bacteria. The raw WAS was firstly adjusted pH level to 3.0 ±0.03 by 1 M of HCl solution and stored at 4°C in a fridge for 24h. Then, the pH level of acidified WAS was adjusted back to 7.0 ±0.03 by 1 M of NaOH solution. After that, 350 mL acid pretreated WAS was mixed with 0.4 g glucose as the carbon source for bacteria and 50 mL trace element solution (as listed in Table 3.2) in a 500 mL Schott Duran bottle. Nitrogen gas was injected into the reactor to maintain the anaerobic condition. The acclimation operation was conducted at 35 ± 1°C for 4 days. And the acclimated WAS was used as the inoculum for biohydrogen fermentation in this study.

Biohydrogen fermentation experiments of TiO_2 photocatalysis pretreated WAS were performed to evaluate the efficiency of photocatalytic pretreatment for enhancing biodegradability of WAS. A number of 500 mL Schott Duran bottles were used as bioreactor for the biohydrogen fermentation experiments. Hydrogen fermentation was performed in four bioreactors using 10-fold diluted WAS without pretreatment and with 12-h pretreatments by TiO_2 adsorption, UV photolysis and TiO_2 photocatalysis as the substrates, respectively. Each bioreactor contains 240 mL pretreated WAS, 120 mL acclimated inoculum sludge and 40 mL trace element solution. Nitrogen gas was injected into the reactor to maintain the anaerobic condition. The biohydrogen fermentation experiments were performed in batch mode at $35 \pm 1^o C$ for 4 days. The biogas was collected using two 50 mL plastic syringes, and the volume was read directly from the scale on the syringe. The gas composition was determined by a gas chromatography. Duplicate experiments in each group were carried out under the same condition, and the mean values were used for analysis.

2.2.5 Analytic methods

The concentration of protein was determined by the coomassie brilliant blue method with bovine serum albumin (BSA) as standard [56]. The pH value was measured using a pH meter (SG8-ELK, SevenGo pro). The TS, VS, COD and NH_4^+-N of the WAS were detected according to the standard methods [57]. Soluble fractions of WAS were defined as passing a 0.45 μm glass microfiber filter. The filtrate was analyzed for soluble COD and soluble protein. The gas composition was

detected using a gas chromatography (GC-8A, SHIMADZU, Japan) using a machine equipped with a thermal conductivity detector and a Porpapak Q column.

2.3 Results and discussion

2.3.1 Protein degradation by TiO$_2$ adsorption, UV photolysis and TiO$_2$ photocatalysis

The photocatalytic degradation of protein was performed under different experimental conditions and the results are illustrated in Fig. 2.1. With 0.5-h dark reaction, protein was approximately 6.3% removed from the buffer solution by the adsorption of TiO$_2$ nanoparticles. This adsorption facilitates the consequent photocatalytic degradation of proteins because an efficient photocatalytic oxidation of target organics requires adsorption onto the surface of TiO$_2$ particles. After 12-h UV irradiation, the removal ratio of protein by TiO$_2$ photocatalysis reached 98.1% which was obviously higher than those by TiO$_2$ adsorption (15.9%), UV photolysis (27.5%) and the control (4.5%). The results indicated that TiO$_2$ photocatalysis effectively improved the nonenzymatic degradation of proteins.

Proteins are hydrolyzed firstly during the degradation to peptides and individual amino acids which are in turn oxidatively degraded to carboxylic acids and ammonia. This can be validated by the decreased pH level and increased ammonium concentration of the suspension with TiO$_2$ photocatalysis. During 12-h UV irradiation, pH levels of the suspensions with TiO$_2$ photocatalysis and UV photolysis continuously decreased from 6.46 to 5.01 and 6.37, respectively. The concentration

of ammonium generated by 12-h TiO$_2$ photocatalytic degradation of proteins reached to 13.5 mg L^{-1} which was higher than that by UV photolysis (shown in Fig. 2.2). The results indicated that TiO$_2$ photocatalysis exhibited higher efficiency than UV photolysis for improving the nonenzymatic degradation of proteins to carboxylic acids and ammonia. Photocatalytic oxidation changes the conformation of proteins and causes peptide hydrolysis [54]. The cleavage of peptide is occurring to form free carboxylic acids and ammonia.

The photocatalytic degradation kinetic of proteins was analyzed by Langmuir-Hinshelwood model [58] which is the most commonly used model to explain the kinetics of heterogeneous photocatalytic processes. This model can be expressed as follows:

$$r = -\frac{dC}{dt} = \frac{k_r \, K \, C}{\left(1 + KC\right)} \tag{2-1}$$

Where r (mg L^{-1} min^{-1}) represents the reaction rate that changes with time t (min); k_r is the limiting rate constant of reaction at maximum converge under the given experimental conditions; K is the equilibrium constant for adsorption of the target organics onto catalyst; C (mg L^{-1}) is the concentration at time t during degradation. Since the term $KC \ll 1$, Eq. (2-1) can be simplified to a first order kinetics and is given by:

$$\ln\left(\frac{C_0}{C}\right) = k_r K t = K_{app} t \tag{2-2}$$

Herein, C_0 (mg L^{-1}) represents the initial concentration of target organics, K_{app} (min^{-1}) is an apparent rate constant for the photocatalytic degradation of organics. As shown

in Fig. 2.3, the high R^2 value (0.988) of the kinetic curve exhibits that TiO_2 photocatalytic degradation of proteins well followed the Langmuir-Hinshelwood kinetic model. The apparent reaction rate constant (K_{app}) calculated from the regression equation is 5.43×10^{-3} min^{-1}. The generation rate of ammonium calculated by the linear regression (as shown in Fig. 2.3) is 0.02 mg L^{-1} min^{-1}.

2.3.2 Effect of TiO_2 dosage on the photocatalytic degradation of proteins

The photocatalytic degradation efficiency of proteins under various TiO_2 dosages is described in Fig. 2.4. Both the degradation ratio and apparent rate constant (K_{app}) increase up to a maximum values with increasing TiO_2 dosage, and then decrease as further increasing the dosage. As shown in Fig. 2.4, increasing the TiO_2 dosage up to 5.0 mg L^{-1} obviously increases the protein degradation. The increase of TiO_2 dosage provides more available active sites on the photocatalyst surface at which proteins can be adsorbed. In addition, the increased amount of TiO_2 photocatalyst produces more oxidative radicals under UV irradiation, which are sufficient and readily accessible for the degradation of nearby protein molecules. However, further increasing the TiO_2 dosage from 5.0 mg L^{-1} to 10.0 mg L^{-1} decreases the protein degradation. This phenomenon can be ascribed to the reduction of active surface area available for protein adsorption and UV photons absorption caused by the aggregation of high-concentration TiO_2 nanoparticles. Additionally, the higher concentration of TiO_2 nanoparticles reduces the penetration intensity of UV light due to the scattering effect [59]. The optimal TiO_2 dosage for the photocatalytic degradation of proteins was 5.0 mg L^{-1} under 2.4 w m^{-2} UV light

irradiation. Since the maximum degradation ratio (98.1%) and K_{app} value (5.27×10^{-3} min^{-1}) were both achieved with 5.0 mg L^{-1} TiO$_2$ dosage, the following experiments were performed at this dosage.

2.3.3 Effect of UV light intensity on the photocatalytic degradation of proteins

The photocatalytic degradation of proteins under different intensity of UV light irradiation with 5.0 mg L^{-1} TiO$_2$ dosage was investigated. Fig. 2.5 presents the effect of UV light intensity on the photocatalytic degradation efficiency of proteins. The photocatalytic degradation efficiency of proteins increases with increasing UV light intensity. The maximum degradation ratio (100%) of proteins is achieved when the UV light intensity increases up to 4.1 w m^{-2}, then further increasing UV light intensity results a slight increase of K_{app} value to 6.78×10^{-3} min^{-1}. The increased UV light intensity induces an increasing amount of UV photons absorbed by TiO$_2$ photocatalyst, and then increases the photoproduced oxidative radicals. That contributes to an increase of photocatalytic degradation efficiency of proteins. For a given TiO$_2$ dosage, since the amount of photocatalytic sites and the transmittance of UV light in the suspension system are constant, unlimited increase of photocatalytic degradation efficiency with continuous increasing of UV light intensity is impossible. Taking energy consumption into account, the optimum UV light intensity for photocatalytic degradation of proteins with 5.0 mg L^{-1} TiO$_2$ dosage is 2.4 w m^{-2} in this study.

2.3.4 TiO$_2$ photocatalytic hydrolysis of waste activated sludge

The major obstacle in TiO_2 photocatalytic pretreatment of WAS is the inhibited UV light transmission caused by its deep color and high-concentration suspended solid characteristics. To enhance the penetration efficiency of UV light, the raw WAS was diluted using deionized water with the dilution ratio of 5, 10, and 15-fold. The photocatalytic pretreatment of raw WAS and diluted ones were performed with TiO_2 dosage of 5.0 mg/L and UV light intensity of 5.0 w m^{-2} by a series of batch experiments.

Fig. 2.6 illustrates the effect of dilution ratio on the photocatalytic pretreatment efficiency of WAS. The COD removal ratio of WAS increase with increasing dilution ratio up to 10-fold, and then decrease with further increasing the dilution ratio. After 12-h pretreatment, the COD removal ratio of raw WAS and diluted WAS with the dilution ratio of 5, 10 and 15-fold were 6.0%, 15.2%, 60.3% and 50.5%, respectively. The ratio of soluble COD (sCOD) to total COD (tCOD) exhibits the same variation trend as COD removal ratio and achieves the maximum value (92.8%) with the dilution ratio of 10-fold. Increasing dilution ratio enhances the penetration intensity of UV light in the suspension system, this results to more oxidative radical generation near active photocatalytic sites on the surface of TiO_2 photocatalysts. Although further increasing dilution ratio continuously increases the penetration of UV light in suspension system, the photocatalytic degradation efficiency decrease due to a reduced ratio of organic substances to TiO_2 photocatalysts.

The main characteristics of 10-fold diluted WAS before/after 12-h pretreatment are listed in Table 2.1. The sCOD/tCOD ratio of WAS pretreated by TiO_2

photocatalysis, UV photolysis and TiO$_2$ adsorption and that of the control were 92.8%, 32.5%, 18.0% and 16.6%, respectively. The results exhibit that TiO$_2$ photocatalysis in comparison with other pretreatments obviously accelerated the hydrolysis of WAS. The decreased pH level from 6.88 to 5.72 by TiO$_2$ photocatalysis indicted that photocatalytic pretreatment of WAS improved the hydrolysis of its macromolecular components such as proteins to carboxylic acids. The increased ratio of soluble protein to total protein from 7.2% to 78.3% provides an evidence for this improvement. The protein degradation ratio of WAS pretreated by TiO$_2$ photocatalysis was 87.0%. Ammonia as one of the main products of protein degradation reached the maximum concentration (23.8 mg L^{-1}) by TiO$_2$ photocatalytic pretreatment of 10-fold diluted WAS. In conclusion, TiO$_2$ photocatalytic pretreatment accelerates the hydrolysis of macromolecular components of WAS to smaller molecular weight hydrolysates which are more readily metabolized by microorganisms in consequent anaerobic digestion.

2.3.5 Biohydrogen production from TiO$_2$ photocatalysis pretreated waste activated sludge

To evaluate the efficiency of photocatalytic pretreatment for enhancing biodegradability of WAS, a series of mesophilic biohydrogen fermentation experiments of TiO$_2$ photocatalysis pretreated WAS were carried out. The performance of biohydrogen production from TiO$_2$ photocatalysis pretreated WAS was compared with that from UV photolysis and TiO$_2$ adsorption pretreated WAS.

Fig. 2.7 shows the cumulative biohydrogen production from pretreated WAS.

The bioreactors containing UV photolysis and TiO_2 adsorption pretreated WASs and the control reactor require 12-h, 21.6-h and 16.8-h start-up period for biohydrogen production, respectively. UV photolysis pretreatment slightly accelerated the biohydrogen production from WAS, while TiO_2 adsorption pretreatment inhibited the biohydrogen production. In contrast, the bioreactor containing TiO_2 photocatalysis pretreated WAS obtained a hydrogen yield of 0.5 mL-H_2/g-VS merely after 12-h mesophilic fermentation. TiO_2 photocatalytic pretreatment obviously accelerated the biohydrogen production from WAS. After 96-h mesophilic fermentation, the cumulative yields of biohydrogen produced from WASs pretreated by UV photolysis and TiO_2 adsorption and the control were 5.2, 1.8 and 6.1 mL-H_2/g-VS, respectively. The cumulative biohydrogen production of control is higher than that of TiO_2 adsorption. In the pretreatment of WAS by TiO_2 adsorption, the nano-sized photocatalysts are prone to adsorption on the surface of particulate substrates and microbial cells. That retards the contact between enzymes/microorganisms and organic substrates, thereby inhibits the biodegradation of WAS and the biohydrogen production. The cumulative biohydrogen production from TiO_2 photocatalysis pretreated WAS reached 11.7 mL-H_2/g-VS, which is 1.9-fold and 2.2-fold of that from the UV photolysis pretreated WAS and the control. The higher yield of biohydrogen produced from TiO_2 photocatalysis pretreated WAS can be ascribed to the enhanced biodegradability of WAS via accelerating the hydrolysis of macromolecular components to smaller molecule weight hydrolysates.

2.4 Summary

The effects of TiO_2 photocatalysis on the hydrolysis of proteins of waste activated sludge and its biodegradability were investigated. It can be concluded from the results that (1) TiO_2 photocatalysis improved the nonenzymatic degradation of protein to carboxylic acids and ammonia. The optimal condition for photocatalytic degradation of protein is TiO_2 dosage of 5.0 mg L^{-1} under 2.4 w m^{-2} UV light irradiation; (2) The hydrogen production from TiO_2 photocatalysis pretreated WAS after 96-h mesophilic fermentation reached 11.7 mL-H_2/g-VS, which was approximately 2.2 times of that from the control; (3) TiO_2 photocatalytic pretreatment of WAS obviously accelerated the hydrolysis of its macromolecular components and improved the hydrogen production in the subsequent biohydrogen fermentation.

Table 2.1 Main characteristics of Raw WAS and 10-fold diluted WAS before/after pretreatment (mean values).

General property	Raw WAS	10-fold diluted WAS				
		initial	after 12-h pretreatment			
			Control	TiO$_2$ adsorption	UV photolysis	TiO$_2$ photocatalysis
pH	6.55	6.88	6.85	6.93	6.54	5.72
TS (mg L^{-1})	8450	840	795	763	615	320
VS (mg L^{-1})	6430	659	605	590	488	265
tCOD (mg L^{-1})	10596	980	898	876	722	389
sCOD (mg L^{-1})	672	74	149	158	235	361
sCOD/tCOD (%)	6.3	7.5	16.6	18.0	32.5	92.8
Total protein (mg L^{-1})	646.0	63.8	61.5	58.6	48.2	8.3
NH$_4^+$-N (mg L^{-1})	119.0	10.7	10.0	8.5	17.1	23.8

Table 2.2 The chemical composition of trace element solution for biohydrogen fermentation

Chemicals	Concentration (g L^{-1})	Chemicals	Concentration (g L^{-1})
NH$_4$Cl	0.5	NaHCO$_3$	4.0
MgCl$_2$ 6H$_2$O	0.085	KH$_2$PO$_4$	0.5
CaCl$_2$ 2H$_2$O	0.01	K$_2$HPO$_4$	0.5
FeCl$_2$ 4H$_2$O	0.15	ZnSO$_4$ 7H$_2$O	0.01
MnCl$_2$ 4H$_2$O	0.03	H$_3$BO$_3$	0.03
CoCl$_2$ 6H$_2$O	0.02	Na$_2$MoO$_4$ 2H$_2$O	0.03
NiCl$_2$ 6H$_2$O	0.02		
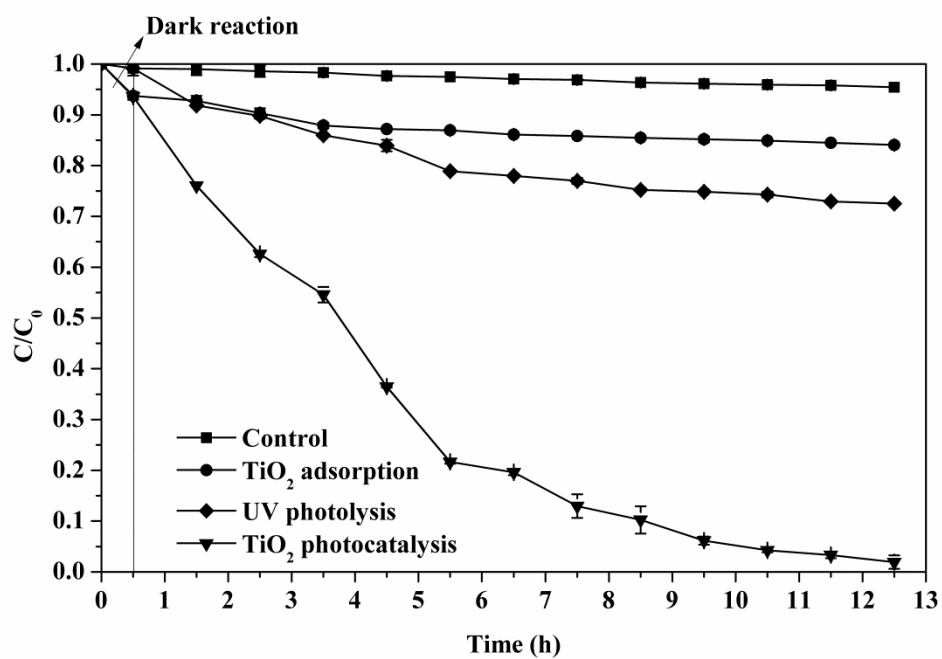
Fig 2.1 Protein degradation by TiO_2 adsorption, UV photolysis and TiO_2 photocatalysis. (Experimental conditions: TiO_2 dosage: 5.0 mg L^{-1}, UV light intensity: 5.0 w m^{-2}, BSA concentration: 500 mg L^{-1})
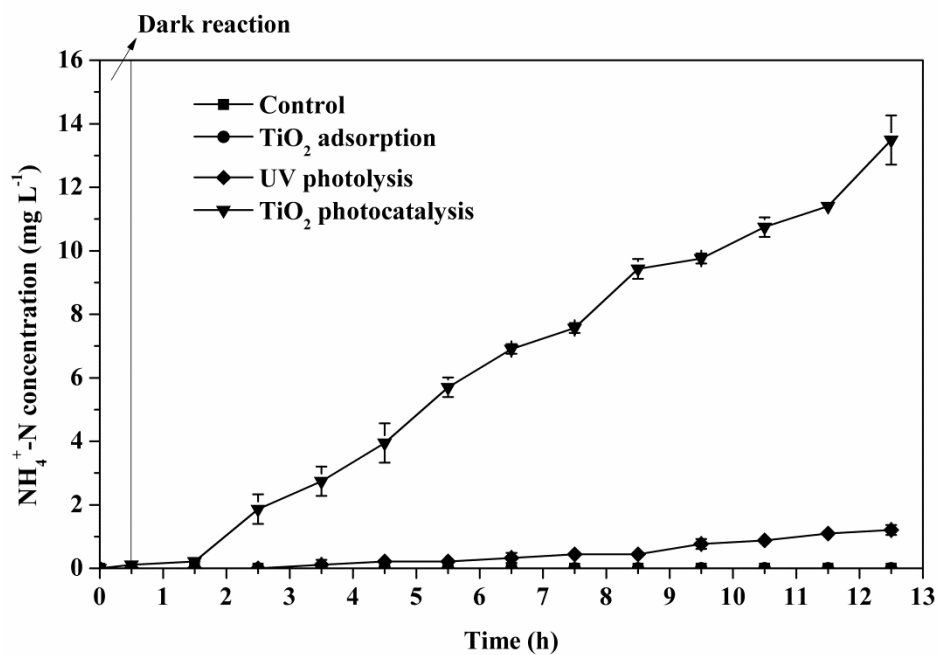
Fig 2.2 The concentration of ammonium generated from the degradation of proteins by TiO_2 adsorption, UV photolysis and TiO_2 photocatalysis.

(Experimental conditions: TiO_2 dosage: 5.0 mg L^{-1}, UV light intensity: 5.0 w m^{-2}, BSA concentration: 500 mg L^{-1})
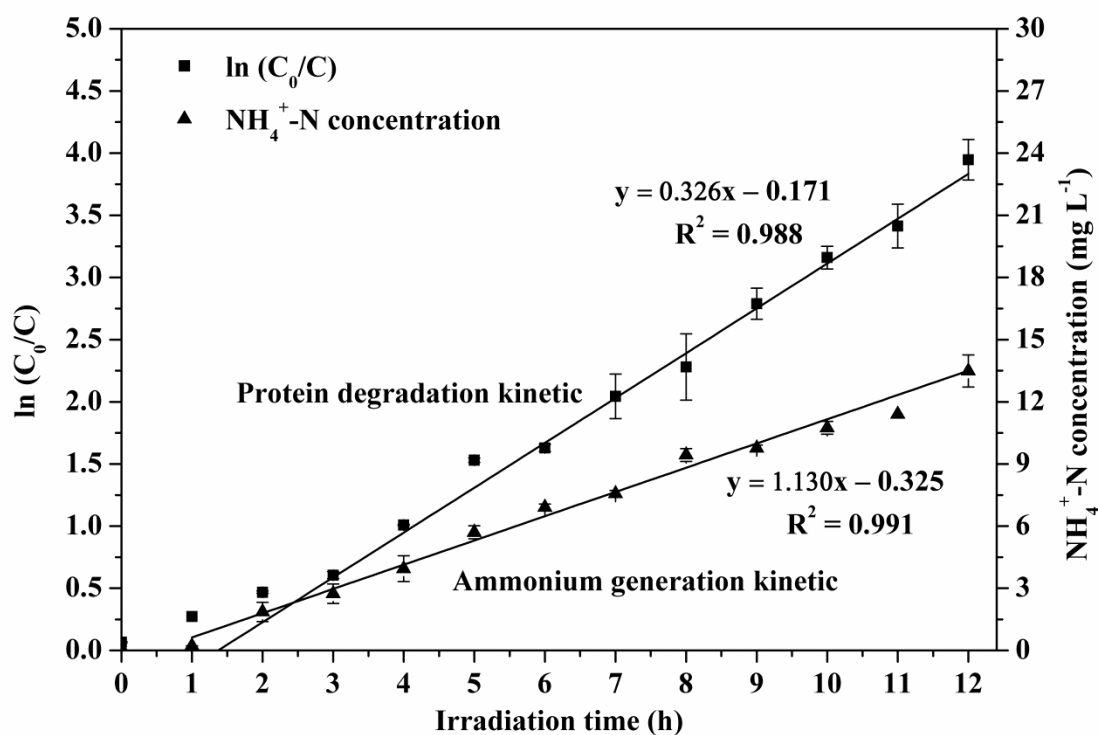
Fig 2.3 Kinetics of protein degradation and ammonium generation during 12-h TiO_2 photocatalysis.

(Experimental conditions: TiO_2 dosage: 5.0 mg L^{-1}, UV light intensity: 5.0 w m^{-2}, BSA concentration: 500 mg L^{-1})
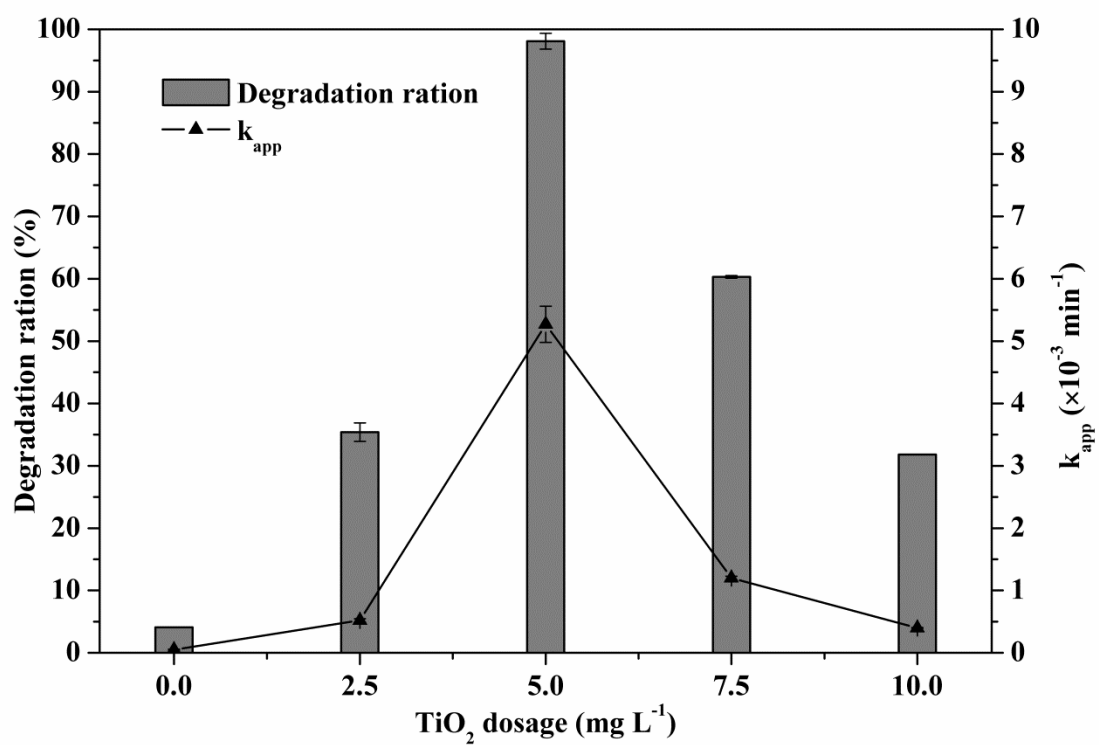
Fig 2.4 Effects of TiO_2 dosage on the degradation ratio and k_{app} value of protein photocatalysis. (Experimental conditions: TiO_2 dosage: 0, 2.5, 5.0, 7.5, 10.0 mg L^{-1}, UV light intensity: 5.0 w m^{-2}, BSA concentration: 500 mg L^{-1})
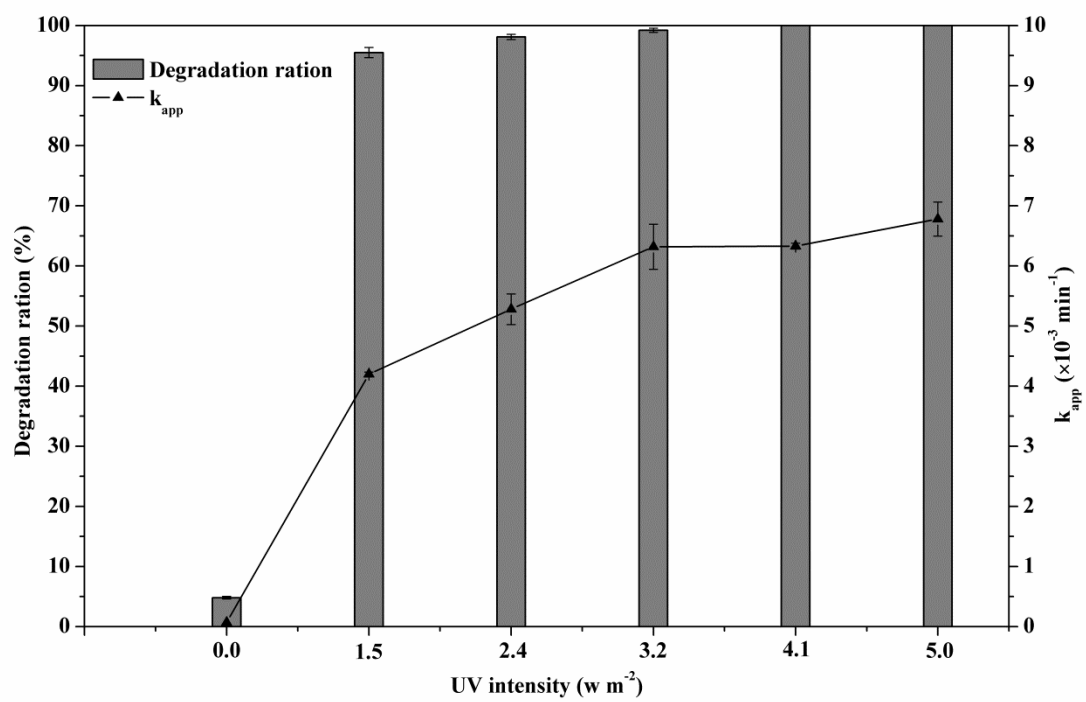
Fig 2.5 Effects of UV intensity on the degradation ratio and k_{app} value of protein photocatalysis. (Experimental conditions: TiO$_2$ dosage: 5.0 mg L^{-1}, UV light intensity: 0, 1.5, 2.4, 3.2, 4.1, 5.0 w m^{-2}, BSA concentration: 500 mg L^{-1})
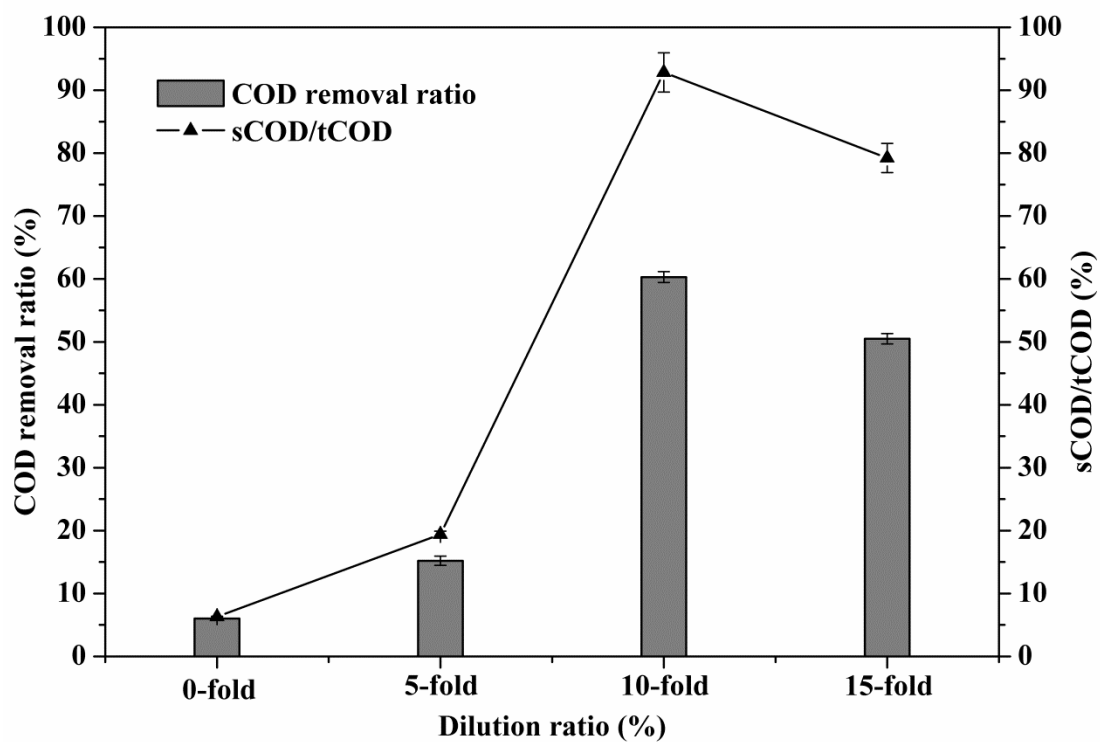
Fig 2.6 Effect of dilution ratio on the hydrolysis of waste activated sludge.
(Experimental conditions: TiO$_2$ dosage: 5.0 mg L^{-1}, UV light intensity: 5.0 w m^{-2}, WAS volume: 120 mL)
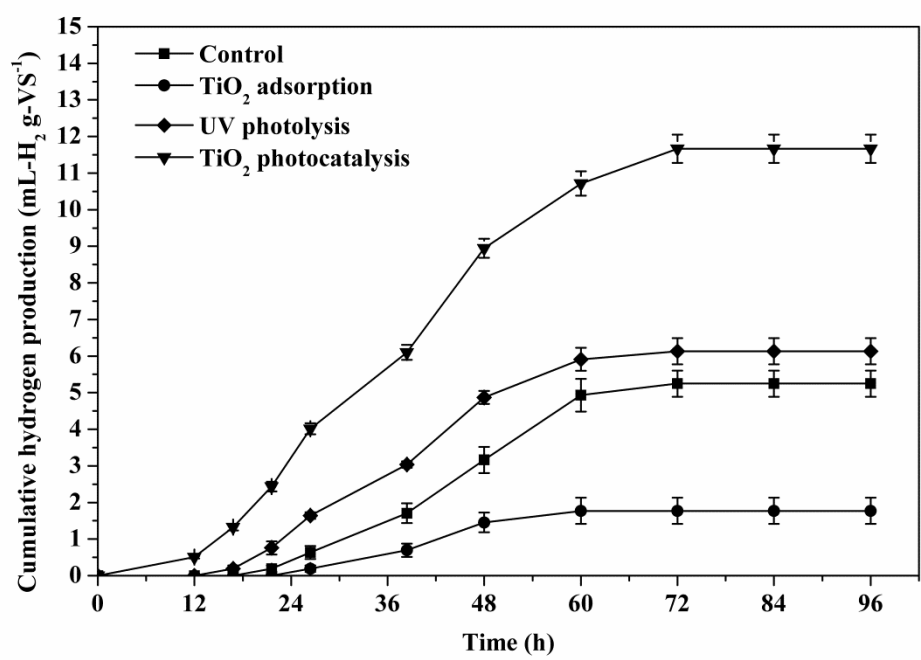
Fig 2.7 Cumulative hydrogen production from TiO$_2$ photocatalysis pretreated waste activated sludge.

Chapter 3 Development of TiO$_2$-coated beads immobilized photocatalytic

reactor for decomposing recalcitrant organic pollutants

3.1 Introduction

Water is one of the most essential substances for existence of life including human beings on the earth. Nevertheless, the contamination of water caused by recalcitrant organic pollutants, such as organic dyes, pesticides and antibiotics, affects seriously the quality of water resource and human health. The decomposition of these organic contaminants is of great significance to the water purification and conservation. Traditional physicochemical remediation processes like adsorption, filtration, flocculation and extraction merely transfer the organic contaminants from one phase to another phase requiring a further treatment [60]. The biological degradation has been found inefficient in remediating the wastewater containing recalcitrant organic contaminants [61, 62]. Consequently, alternative advanced technologies are required for the decomposition of recalcitrant organic contaminants in wastewater.

During the last decades, advanced oxidation processes (AOPs) have attracted considerable attention for decomposing recalcitrant and non-biodegradable organic pollutants. Heterogeneous photocatalysis superior to other AOPs is a promising technology since the easy operation under ambient temperature and pressure [63]. Titanium dioxide (TiO$_2$) has been proven to be the most suitable photocatalyst due to its high chemical stability, strong photocatalytic activity, inexpensive and nontoxicity

[64, 65]. TiO_2 photocatalysis has been demonstrated to be an effective technique for the degradation of recalcitrant organics in wastewater [66-69]. However, its practical application for wastewater treatment is constrained by several technical challenges, i.e. light penetration, mass transfer and electron-hole recombination [70, 71], all of which need to be further investigated.

The development of photocatalytic reactor, as well as synthetizing photocatalyst, has been systematically investigated for a successful application of TiO_2 photocatalysis in wastewater treatment. There are generally two types of photocatalytic reactor configurations: slurry suspension system (TiO_2 nanoparticles being suspended in the aqueous phase) and catalyst immobilization system (TiO_2 nanoparticles being fixed to a substrate) [72]. Currently used photocatalytic reactor for liquid phase oxidation is typically based on the slurry suspension system. Although the slurry type photocatalytic reactor exhibits several advantages such as simple reactor configuration and high surface area for adsorption and reaction, its low light utilization efficiency and difficult separation/recovery of nano-sized photocatalysts after the reaction [73] lead to a low effectiveness and high cost of this design. In addition, recent studies have raised concerns about the potential toxicity of TiO_2 nanoparticles [74, 75]. In order to overcome the deficiency of slurry suspension system, the immobilization of photocatalysts on a support or within the photoreactor has attracted increasing concern in recent years. Nano-sized TiO_2 particles can be immobilized on various support substrates including glass [76, 77], stainless [78, 79], alumina [80], activated carbon [81, 82] and zeolite [83, 84] using many different

coating techniques such as sol-gel [85, 86], chemical deposition [87, 88] and magnetron sputtering [89]. Activated carbon and zeolite, which possessing high adsorption capacity, are usually considered as an excellent catalyst support because the efficient photocatalytic oxidation of target organics requires adsorption onto the surface of TiO_2 particles. Nevertheless, the inherent light-tight property of these two support materials retards the photon transmission in a photocatalytic reactor, thereby lowers the light utilization efficiency. In terms of immobilizing photocatalysts within the photoreactor, several novel photocatalytic reactors characterized respectively by UV-LED/TiO_2 coated quartz tube [60], TiO_2 coated capillary array inserting with UV lamp [90] and TiO_2 immobilized cylindrical reactor inserted with UV-LED [91] have been developed for wastewater treatment. However, the loss of photocatalytic activity caused by shedding of immobilized catalysts, the lower active surface accessible to the target pollutants, and low light utilization efficiency are still remain the major bottlenecks of catalyst immobilized system. For promoting the efficiency of catalyst immobilization system, there is great need to search a high-translucency support material possessing high adsorption capacity and/or modify the configuration of photocatalytic reactor.

In this study, a novel TiO_2-coating beads immobilized photocatalytic reactor (TBIPR) was developed to overcome the obstacles present in catalyst immobilized systems. The primary objectives of this work are to investigate the photocatalytic efficiency and repetitive operation performance of developed TBIPR for the decomposition of recalcitrant organic contaminants in wastewater. The

photocatalytic efficiency and repetitive operation performance of TBIPR was investigated by monitoring its Rhodamine B (RhB) degradation performance in a series of continuous experiments.

3.2 Materials and methods

3.2.1 Reagents and materials

Organic dyes are one of the most contaminants widely found in wastewaters because of their huge volume of production from industries, slow biodegradation and toxicity. Rhodamine B (RhB) is a representative organic dye used extensively in the printing, textile and photographic industries, due to their good water-solubility, high stability and bright color. RhB obtained from Wako Pure Chemical Industries, Ltd. (Osaka, Japan) was chosen as the target recalcitrant organic pollutants to evaluate the photocatalytic performance of developed TBIPR in this study. Its molecular structure and chemical properties are described in Table 3.1. Deionized water was used to prepare all the experimental solutions.

TiO_2-coated beads newly developed by Photocatalytic Materials Research Institute (Nagoya, Japan) were employed as the photocatalysts to be fixed on the photoreactor. Alumina (Al_2O_3) beads without photocatalytic activity supplied by Ikeda Scientific Co, Ltd (Tokyo, Japan) were used as the control of TiO_2-coated beads. The physicochemical properties of TiO_2-coated beads and Al_2O_3 beads are described in Table 3.2.

3.2.2 TiO_2-coated beads immobilized photocatalytic reactor (TBIPR)

For enhancing the light utilization efficiency, a pair of cylindrical-shell photoreactors (height: 350 mm; external diameter of interior glass tube: 60 mm; internal diameter of exterior plexiglass tube: 84 mm; thickness of each tube: 3 mm) each inserted axially with an UV black light lamp (length: 300 mm; diameter: 28 mm; power: 10 w) were designed in this study. The axial distribution of UV light in the cylindrical shell of each photoreactor is heterogeneous. The UV light intensity at the top, middle and bottom of each photoreactor is 6.3, 17.6 and 6.5 w m^{-2}, respectively. The average UV light intensity in the cylindrical shell of the photoreactor is 10 w m^{-2}. A number of newly developed TiO$_2$-coated beads (diameters: 2-3 mm) were fixed to the external surface of interior glass tube of one cylindrical-shell photoreactor to form the TBIPR. The control reactor was constructed by immobilizing numerous Al$_2$O$_3$ beads (diameters: 2-3 mm) to the same position of the other cylindrical-shell photoreactor. The working volume of the developed reactors is 800 mL. The whole photocatalytic system (shown in Fig. 3.1) consists of following three parts: a liquid storage tank (volume capacity: 500 mL) with one magnetic stirrer (SRS116AA, ADVANTEC, Japan), a recirculation pump (PA26A, Masterflex, USA) and the developed TBIPR.

3.2.3 Removal of RhB by UV photolysis, TiO$_2$-coated beads adsorption and TiO$_2$ photocatalysis

The removal of RhB was performed using developed control reactor and TBIPR under different experimental conditions including (i) control, (ii) UV photolysis, (iii) TiO$_2$-coated beads adsorption and (iv) TiO$_2$ photocatalysis. Turn off/on the UV lamp

of control reactor, what means without/with UV irradiation, corresponding to the conditions of control and UV photolysis. The same operations of developed TBIPR correspond to the conditions of TiO_2-coated beads adsorption and TiO_2 photocatalysis.

The prepared 1200 mL of RhB (5 mg L^{-1}) solution was taken in a conical flask (volume capacity: 2000 mL) and passed through the reactor inlet. Then, the dye solution was continuously circulated through the reactor and liquid storage tank with magnetic stirring at the flow rate of 50 mL min^{-1} by a recirculation pump, 4 mL of degraded sample was withdrawn at every half hour up to 12 h. The concentrations of RhB in all samples were determined using a calibration curve of RhB solution (concentration vs absorbance) prepared separately with known concentration from UV-visible spectra. Absorbance measurement was done using an UV-visible spectrophotometer (UV1800, SHIMADZU, Japan) at 554 nm. The adsorption spectrum of RhB was recorded on a UV-VIS-NIR scanning spectrophotometer (UV-3100PC, SHIMADZU, Japan) in the 200-800 nm wavelength range. Duplicate experiments were conducted under every condition, and the mean values were used for analyses.

3.2.4 Optimization of developed TBIPR parameters for RhB degradation

In the application of any designed photocatalytic reactor for the decomposition of environmental contaminants, flow rate and initial concentration of target organics play important roles for a complete decontamination. In this study, the photocatalytic degradation of RhB (10 mg L^{-1}) solution was carried out using the developed TBIPR

with different flow rates: 20, 35, 50, 65 and 80 mL min^{-1}. The effect of initial RhB concentration on the photocatalytic performance of developed TBIPR with the flow rate of 50 mL min^{-1} was conducted in the range of 2.5-12.5 mg L^{-1}.

Long-term operation performance of developed photocatalytic reactor is of vital importance for its practical application. In the present study, five repetitive operations of developed TBIPR were performed to treat 5 mg L^{-1} RhB solution (1200 mL/operation).

In all the experiments, 4 mL of degraded sample was withdrawn at every half hour up to 12 h, the concentrations of RhB in all samples were measured using a UV-visible spectrophotometer. Duplicate experiments were carried out under the same condition, and the mean values were used for analyses.

3.2.5 Energy consumption for RhB and MO degradations using developed TBIPR

Energy consumption is an essential parameter to evaluate the efficiency of photocatalytic oxidation process. In order to calculate the energy consumption of developed TBIPR and compare with reported reactors, the same concentration (10 mg L^{-1}) of RhB and MO solutions (1200 mL) were treated, respectively. The sampling and measurement methods are the same as previously described.

3.2.6 Analytic methods

The specific surface areas and pore size distributions of TiO$_2$-coating beads and Al$_2$O$_3$ beads were determined by N$_2$ adsorption using a Brunauer-Emmett-Teller

(BET) specific surface area analyzer (SA3100, Coulter, USA). The morphological features of TiO_2 coating beads and Al_2O_3 beads were analyzed by a scanning electron microscope (SEM) (JSM-6330F, JEOL, Japan). The UV light intensity of the developed photoreactors was measured by an UV light meter (UV340, CUSTOM, Japan). The absorbance measurement of RhB solution was carried out using an UV-visible spectrophotometer (UV1800, SHIMADZU, Japan) at 554 nm. The adsorption spectrum of RhB was recorded on a UV-VIS-NIR scanning spectrophotometer (UV-3100PC, SHIMADZU, Japan) in the wavelength range of 200-800 nm.

3.3 Results and discussion

3.3.1 BET surface area and SEM analysis of TiO_2-coated beads and Al_2O_3 beads

The BET surface area of TiO_2-coated beads and Al_2O_3 beads were measured by N_2 adsorption isotherm analysis. The measured BET surface area of TiO_2-coated beads was 118.43 m^2 g^{-1} with pore volume of 0.80 cm^3 g^{-1}, which was much higher than that of Al_2O_3 beads (2.33 m^2 g^{-1}). Pore size distribution of the TiO_2-coated beads was presented in Fig. 3.2. The pores of TiO_2-coated beads are mainly between 20-80 nm, indicating that it is a mesoporous material according to the classification of porous materials by International Union of Pure an Applied Chemistry (IUPAC). The high specific surface area and abundant mesoporous structure is likely to enhance the adsorption capacity of target organics, and thereby facilitate their photocatalytic degradation on the surface of TiO_2-coated beads. By contrast, Al_2O_3

beads seem to be a suitable control material for TiO_2-coated beads due to its low specific surface area and poor porous structure besides non-photocatalytic activity.

The TiO_2-coated beads used in this study was synthesized by immobilizing TiO_2 nanoparticles on the surface of silica beads. The morphology of TiO_2-coated beads and its silica carrier as well as the Al_2O_3 beads was observed by SEM analysis. Fig. 3.3a and b shows the SEM images of the silica carrier and TiO_2-coated beads. The silica carrier exhibits a rough and porous surface, which contributes partially a high specific surface area and abundant porous structure to the TiO_2-coated beads. After the immobilization of TiO_2 nanoparticles, a lots of TiO_2 clusters formed on the surface of silica carrier, that enables the material possessing photocatalytic activity. As shown in Fig. 3.3c, the surface of Al_2O_3 beads is much smooth and none TiO_2 cluster can be observed in comparison with the TiO_2-coated beads. That is the reason of using Al_2O_3 beads as a control material for the TiO_2-coated beads in this study.

3.3.2 Characteristics of TiO_2-coated beads immobilized photocatalytic reactor (TBIPR)

The developed TBIPR consists of a cylindrical-shell structural unit, numerous TiO_2-coated beads and a UV black light lamp (as shown in Fig. 3.1). The UV lamp pipe was inserted axially to obtain maximum irradiation on the TiO_2-coated beads immobilized on the cylindrical-shell structure. On the other hand, the high-translucency characteristic of TiO_2-coated beads increases the penetration intensity of UV light due to its lower scattering effect in comparison with TiO_2 coated zeolite [84] and activated carbon [82]. The average UV light intensity in the

cylindrical shell of developed TBIPR is 10 w m^{-2}. In addition, the total surface area of spherical TiO$_2$-coating beads is much higher than that of general TiO$_2$ coated quartz tube. The calculated total surface area of TiO$_2$-coating in developed TBIPR was 3.3 times of that in TiO$_2$ coated quartz tube. This increases the contact area between UV photons and TiO$_2$ nanoparticles. All of these characteristics significantly enhanced the UV light utilization efficiency.

3.3.3 Removal of RhB by UV photolysis, TiO$_2$-coated beads adsorption and TiO$_2$ photocatalysis

The decolorization of RhB was performed under different experimental conditions and the results are shown in Fig. 3.4. After 12-h treatment, the control and UV photolysis (control photoreactor without/with UV irradiation) obtained 10.96% and 16.29% decolorization of RhB, respectively. The decolorization can be ascribed to the adsorption of RhB on Al$_2$O$_3$ beads immobilized on the photoreactor. Enhanced removal of RhB in the later condition was partially resulted by the photolysis under UV irradiation, except for the adsorption on Al$_2$O$_3$ beads. As shown in Fig. 3.4, TiO$_2$-coated beads adsorption and TiO$_2$ photocatalysis (developed TBIPR without/with UV irradiation) achieved 51.67% and 89.46% decolorization of RhB, respectively. The TiO$_2$-coating beads, in comparison with Al$_2$O$_3$ beads, exhibited higher adsorption capacity for RhB due to its high specific surface area and abundant mesoporous structure. The high adsorption capacity of TiO$_2$-coated beads improved the transportation of RhB molecules to the vicinity of photocatalytic sites and thereby facilitated its photocatalytic degradation.

Fig. 3.5a presents the UV-VIS-NIR spectral distribution of RhB after 12-h treatment by UV photolysis, TiO_2-coated beads adsorption and TiO_2 photocatalysis. The peak height of RhB at 554 nm approximately reduced half by TiO_2-coated beads adsorption, but the peak shape remained the same. This result was caused by the transportation of RhB from liquid phase (solution) to solid phase (TiO_2-coated beads) by single adsorption without any degradation. With TiO_2 photocatalysis, not only the peak height of RhB at 554 nm reduced more obviously than single adsorption, but also the peak shape was distinctly difference from its original form. The same change of peaks at 355 and 255 nm can be observed in Fig. 3.5a. The change process of peaks at 554, 355 and 255 nm was illustrated in Fig. 3.5b. Variation of the peak shape demonstrated that TiO_2 photocatalysis effectively degraded the organic compounds in aquatic solution rather than simply transport them from one phase to another phase. The results indicated that both RhB and other organic compounds in aqueous solution were successfully decomposed via TiO_2 photocatalysis using developed TBIPR.

3.3.4 Adsorption kinetics of RhB onto TiO_2-coated beads

Adsorption capacity has a major influence on the efficiency of photocatalytic degradation [92], since adsorption is the primary approach by which organic contaminants are transported to the vicinity of the photocatalytic sites [93]. To understand the mechanisms of RhB adsorption onto TiO_2-coated beads, the pseudo-fist-order and pseudo-second-order kinetic models were used in this study. The adsorption kinetic models can be described as Eq. (3-1) and Eq. (3-2),

respectively.

$$\log\left(q_e - q_t\right) = \log q_e - \frac{k_1 t}{2.303} \tag{3-1}$$

$$\frac{t}{q_t} = \frac{1}{k_2 q_e^2} + \frac{t}{q_e} \tag{3-2}$$

Where q_t and q_e (mg g^{-1}) are the amount of RhB adsorbed on per mass of TiO$_2$-coated beads at time t and equilibrium time, respectively; k_1 and k_2 are the first-order and second-order rate constants for adsorption. The adsorption kinetic of RhB onto TiO$_2$-coated beads were shown in Fig. 3.6a. The obtained experimental data well fit with pseudo-second-order adsorption kinetic model, herein the correlation coefficient (R^2) is 0.988. The calculated adsorption capacity q_e and adsorption rate constant k_2 values according to the linear regression of t/q_t versus t and Eq. (3-2) were 0.0616 mg g^{-1} and 0.0265 g mg^{-1} min^{-1}, respectively.

Besides surface-adsorption, the adsorption process by a porous adsorbent also includes an intra-diffusion step. Intra-particle diffusion model proposed by Weber and Morris [94] was employed to identify the diffusion mechanism of RhB in TiO$_2$-coated beads. This model can be expressed as:

$$q_t = k_i t^{0.5} \tag{3-3}$$

Where k_i (mg g^{-1} h$^{-0.5}$) represents the intra-particle diffusion rate constant. Fig. 4.6b presents the intra-particle diffusion kinetic of RhB into the TiO$_2$-coated beads. The intra-particle diffusion kinetic model described this process very well ($R^2 = 0.997$). The intra-particle diffusion rate constant k_i calculated from the slope of the regression line is 1.15×10^{-2} mg g^{-1} h$^{-0.5}$. The high surface-adsorption and intra-diffusion of RhB on porous TiO$_2$-coated beads is of great important for its

following photocatalytic degradation.

3.3.5 Photocatalytic degradation kinetic of RhB using TBIPR

Langmuir-Hinshelwood (L-H) kinetic model [95] is the most commonly used model to explain the kinetics of heterogeneous photocatalytic processes. In this study, L-H model was employed to explain the photocatalytic degradation kinetic of RhB using developed TBIPR. This model can be expressed as follows:

$$r = -\frac{dC}{dt} = \frac{k_r KC}{(1 + KC)} \tag{3-4}$$

Where r (mg L^{-1} min^{-1}) represents the reaction rate that changes with time t (min); k_r is the limiting rate constant of reaction at maximum converge under the given experimental conditions; K is the equilibrium constant for adsorption of the target organics onto catalyst; C (mg L^{-1}) is the concentration at time t during degradation. Since the term $KC \ll 1$, Eq. (3-4) can be simplified to a first order kinetics and is given by:

$$\ln\left(\frac{C_0}{C}\right) = k_r Kt = k_{app}t \tag{3-5}$$

Where C_0 (mg L^{-1}) represents the initial concentration of target organics, k_{app} (min^{-1}) is an apparent rate constant for the photocatalytic degradation of organics. As shown in Fig. 3.6a, the high R^2 value (0.999) of the kinetic curve exhibits that photocatalytic degradation of RhB using developed TBIPR well followed the L-H kinetic model. The apparent reaction rate constant (k_{app}) calculated from the regression equation is 3.12×10^{-3} min^{-1}.

3.3.6 Effect of flow rate on the photocatalytic degradation of RhB using TBIPR

In this present study, the photocatalytic degradation of RhB (10 mg L^{-1}) was performed with different flow rates (i.e. 20, 35, 50, 65 and 80 mL min^{-1}) using the developed TBIPR. The influence of flow rate on the degradation of RhB was illustrated in Fig. 3.7. The degradation ration of RhB increased from 90.8% to 92.8% with increasing the flow rate from 20 mL min^{-1} to 50 mL min^{-1}, and exhibited a slight fluctuation around 92.8% with further increasing the flow rate from 50 mL min^{-1} to 80 mL min^{-1}. As shown in Fig. 3.7, the corresponding K_{app} values exhibited the same variation trend with flow rate and fluctuated around 3.68×10^{-3} min^{-1}. The results indicated that increasing the flow rate may enhance the degradation of RhB and there exists an optimal flow rate for this enhancement. However, completely contrary results were reported in many literatures [60]. Flow rate affects the photocatalytic reaction mainly by changing the convective mass transfer and contact time in a continuous-flow reactor. Under low flow rate, photocatalytic degradation of target organics is restrained mainly by the convective mass transfer. Increasing flow rate reduces the convective mass transfer resistance of target organics and photocatalytic intermediates thereby facilitates the photocatalytic degradation of organics. With high flow rate, the contact time in comparison with the convective mass transfer is the dominant factor that limits the degradation of target organics. That means increasing the flow rate will decrease the contact time between target organics and immobilized photocatalysts, then lower the photocatalytic degradation of the organics. Consequently, some previous study [60, 96] concluded that

51

increasing the flow rate decreases the photocatalytic degradation of organics by shortening the contact time. There exists an optimal flow rate for the degradation of target organics using designed continuous-flow photocatalytic reactors. The optimal flow rate for the photocatalytic degradation of RhB using developed TBIPR is 50 mL min^{-1} in this study.

3.3.7 Effect of initial concentration on the photocatalytic degradation of RhB using TBIPR

The effect of initial RhB concentration on its photocatalytic degradation was investigated at different concentrations varying from 2.5 to 12.5 mg L^{-1} using developed TBIPR with the flow rate of 50 mL min^{-1}. As shown in Fig. 4.8, the increase of initial RhB concentration leads to the decrease of photocatalytic degradation ration and k_{app} values. Similar results have been reported concerning the photocatalytic oxidation of RhB under UV/solar light using ZnO nanopowder [97]. The maximum degradation ration (91.70%) and k_{app} value (3.52×10^{-3} min^{-1}) of RhB were obtained at the initial concentration of 2.5 mg L^{-1}. For a designed photocatalytic reactor, since the light irradiation time and the amount of photocatalysts are constant, the photoproduced oxidative species including holes (h_{vb}^{+}), hydroxyl radicals (OH) and superoxide radicals ($O_2 \cdot$) remain practically same. Although increasing initial concentration increases the adsorption amount of target organics on the photocatalysts, the rate of photocatalytic degradation decreases due to a lower ratio of oxidative species to organic molecules [98]. On the other hand, the penetration intensity of light decreases with increasing initial concentration,

which resulting in less active photocatalytic sites creation on the surface of photocatalysts.

3.3.8 Repetitive operation performance of developed TBIPR

Repetitive operation performance is one of the most important parameters in the application of any developed photocatalytic reactor for decomposing recalcitrant organic contaminants in wastewater. To evaluate the repetitive operation performance of developed TBIPR, the photocatalytic degradation of 5 mg L^{-1} RhB (1200 mL) was repeated up to five cycles. After each operation, the developed photocatalytic reactor was washed with 1% (v/v) methanol solution and pure deionized water, respectively. Fig. 3.9 illustrates the photocatalytic degradation of RhB in five repetitive operations. This figure shows that more than 90.0% RhB was decomposed after 12-h photocatalysis in each operation. The five repetitive operations gave a relative standard deviation of 0.32%, indicating that the photocatalytic performance of developed TBIPR remains almost constant. This can be ascribed to the high stability of TiO_2-coated beads immobilized on the photoreactor. Fig. 3.3d shows the SEM image of regenerated TiO_2-coated beads after five repetitive operations. The morphology feature of regenerated TiO_2-coated beads was little changed comparing with that of original ones (shown in Fig. 3.3b), demonstrating the stability of TiO_2-coated beads. The results indicated that the developed TBIPR has an excellent long-term operation performance for the photocatalytic degradation of target organic contaminants in wastewater. The high efficiency of developed TBIPR can be ascribed to its unique design of

cylindrical-shell configuration inserting axially with an UV black light lamp and the high-translucency characteristic of the immobilized TiO_2-coated beads. These properties of developed TBIPR ensure a maximum utilization of the UV light energy thereby greatly decreased its electrical energy consumption. Integrating the low-energy consumption characteristic with its high efficiency and excellent long-term operation performance, it can be concluded that the developed TBIPR is a promising alternative for decomposing recalcitrant organic contaminants in wastewater.

3.3.9 Electrical energy consumption for RhB degradation using developed TBIPR

Energy consumption is an important parameter to evaluate the efficiency of photocatalytic reactor for the degradation of target organics. The energy consumption for the degraded dyes (RhB and MO) using developed TBIPR was calculated. This calculation was based on the electrical energy per mol (E_{em}), defined as the number of kilowatt hours (kWh) of electrical energy required to decompose one mol target organics in per unit time. The E_{em} (kWh mol^{-1} min^{-1}) can be calculated from the following equation:

$$E_{em} = \frac{pt}{\dfrac{CVR}{M}} \times \frac{1}{t} = \frac{pM}{60CVR}$$

(3-6)

Where p (w) is the power input to draw the UV lamp; t (min) is the irradiation time; C (mg L^{-1}) is the initial concentration of target organics; V (L) is the total volume of target organic solutions, R (%) is the degradation ration at time t; M (g mol^{-1}) is the

molar weights of target organics. The E_{em} values for the degradation of RhB and MO using developed TBIPR was 7.36 and 5.39 kWh mol^{-1} min^{-1}, respectively. The values were much lower comparing with other photocatalytic reactors [98, 99]. The energy consumption of developed TBIPR for the degradation of RhB and MO will be compared in detail with reported photocatalytic reactors in the following part.

3.3.10 Comparison of developed TBIPR with reported photocatalytic reactors

The photocatalytic degradation efficiency of different target organics is highly dependent on the experimental conditions such as the types and dosage of photocatalysts, light irradiation source, configurations of photocatalytic reactor and reaction time. The efficiency for different dyes (RhB and MO) photocatalytic degradation by developed TBIPR and other reported photocatalytic reactors are compared in Table 3.3.

The degradation rate of RhB and MO using developed TBIPR was 0.31×10^{-4} and 0.43×10^{-4} mol min^{-1} respectively, which were lower than those of most slurry-type photocatalytic reactors (shown in Table 3.3). This mainly ascribed to the higher surface area of slurry suspension system for the adsorption and reaction. However, the difficult separation/recovery of nano-sized photocatalysts after reaction seriously constrained the practical application of slurry-type photocatalytic reactors. This problem can be solved using developed TBIPR. As shown in Table 3.3, the degradation rates of RhB and MO using developed TBIPR was about 3/4 and 1/2 of those by TiO$_2$ nanotubes thin-film [70] and TiO$_2$ nanoparticles thin-film [101] photocatalytic reactors, respectively. Nevertheless, the corresponding E_{em} values for

the degradation of RhB and MO using developed TBIPR was merely 1/10 and 1/8 of that by these two thin-film photocatalytic reactors, respectively. Actually, the E_{em} values for the degradation of RhB and MO using developed TBIPR was much lower than those by previously reported photocatalytic reactors (shown in Table 3.3). The high efficiency and low-energy consumption of developed TBIPR can be ascribed to its unique design of cylindrical-shell configuration inserting axially with an UV black light lamp and the high-translucency characteristic of the immobilized TiO$_2$-coated beads. These properties of developed TBIPR ensure a maximum utilization of the UV light energy thereby greatly decreased its electrical energy consumption. Integrating the low-energy consumption characteristic with its high efficiency and excellent long-term operation performance, it can be concluded that the developed TBIPR is a promising alternative for decomposing persistent organic contaminants in wastewater.

3.4. Summary

A novel TiO$_2$-coated beads immobilized photocatalytic reactor (TBIPR) was developed and successfully applied for the degradation of Rhodamine B and Methyl Orange. The high adsorption capacity of TiO$_2$-coated beads facilitates the photocatalytic degradation of target organics by improving the transportation of organic molecules to the vicinity of photocatalytic sites. Flow rate affects the photocatalytic reaction mainly by changing the convective mass transfer and contact time in the developed TBIPR. There exists an optimal flow rate for the photocatalytic degradation of target organics using developed TBIPR. The increase

of initial concentration lowers the ratio of oxidative species to organic molecules and the light transmission in the developed TBIPR thereby decreases the photocatalytic degradation of target organics. The stability of TiO_2-coated beads contributes to an excellent repetitive operation performance of the developed TBIPR. The high efficiency and low-energy consumption of developed TBIPR can be ascribed to its unique cylindrical-shell configuration inserting axially with an UV black light lamp and the high-translucency characteristic of the TiO_2-coated beads. The developed TBIPR exhibits high efficiency, low-energy consumption and excellent long-term operation performance. It is a promising alternative for the decomposition of persistent organic contaminants in wastewater using developed TBIPR.

Table 3.1 Molecular structure and chemical properties of the dyes.
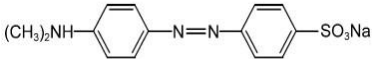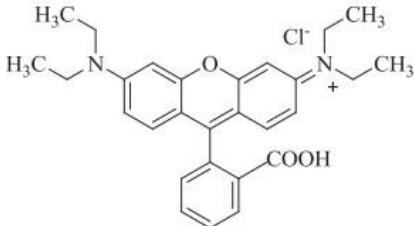
Molecular structure	Chemical properties	
Methyl Orange		
	Chemical formula	$C_{14}H_{14}N_3SO_3Na$
	Molecular weight	327.33 g mol^{-1}
	Absorption maximum	464 nm
	Class	Azo dye
Rhodamine B		
	Chemical formula	$C_{28}H_{31}N_2O_3Cl$
	Molecular weight	479.01 g mol^{-1}
	Absorption maximum	554 nm
	Class	Triphenylmethane

Table 3.2 Physicochemical properties of TiO_2-coated beads and Al_2O_3 beads.

Parameters		TiO_2 beads	Al_2O_3 beads
	TiO_2	20	0
Chemical composition (%)	SiO_2	80	7
	Al_2O_3	0	93
Particle size (mm)		2-3	2-3
BET surface area ($m^2 g^{-1}$)		118.43	2.33
t-Plot surface area ($m^2 g^{-1}$)		106.71	2.46
Micropore surface area ($m^2 g^{-1}$)		12.06	0.00
Micropore volume ($cm^3 g^{-1}$)		0.80	0

Table 3.3 Energy consumption for the photocatalytic degradation of organic dyes (RhB and MO) using developed TBIPR and reported reactors.

Dyes	Concentration (mg L^{-1})	Catalyst	Reactor type	Power input (w)	Degradation rate ($\times 10^{-4}$ mol min^{-1})	E_{em} (kWh mol^{-1} min^{-1})	References
MO	20	CNTs/P-TiO$_2$	Slurry	250	1.53	272.78	[66]
	10	TiO$_2$ nanotubes	Slurry	800	0.97	2282.64	[67]
	15	TiO$_2$/ZnO/Chitosan	Thin-film	300	0.19	1115.64	[99]
	5	TiO$_2$	Thin-film	28	0.91	42.76	[100]
	10	TiO$_2$ beads	Immobilized	10	0.43	5.39	This study
RhB	10	Degussa P-25	Slurry	15	0.98	42.47	[101]
	20	Modified P-25	Slurry	150	0.22	748.45	[102]
	20	Ag/H$_3$PW$_{12}$O$_{40}$/TiO$_2$	Thin-film	300	0.14	2020.12	[103]
	20	TiO$_2$ nanotubes	Thin-film	11	0.41	74.68	[70]
	10	TiO$_2$ beads	Immobilized	10	0.31	7.36	This study
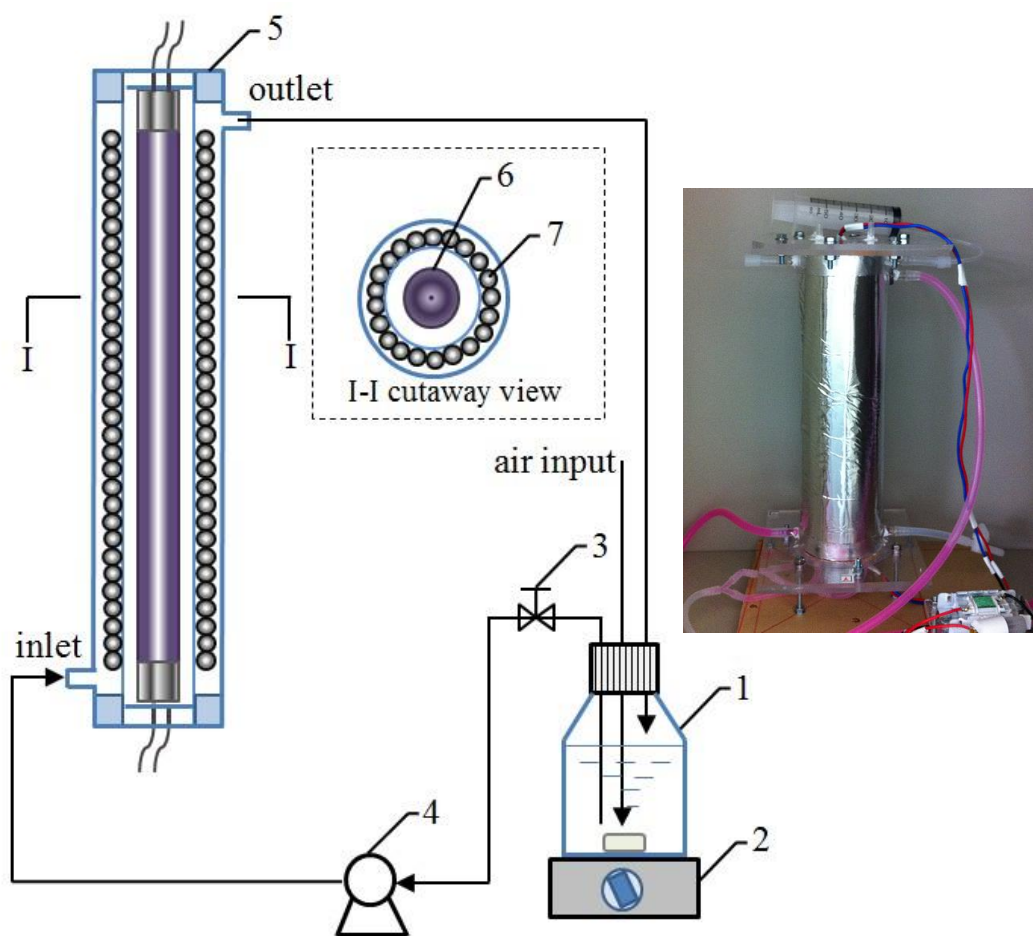
Fig 3.1 The schematic of developed novel photocatalytic system.
(Note: 1–liquid storage tank; 2–magnetic stirrer; 3–sampling valve; 4–peristaltic pump;
5–TiO$_2$-coated beads immobilized photocatalytic reactor; 6–UV light lamp; 7–TiO$_2$-coated
beads)
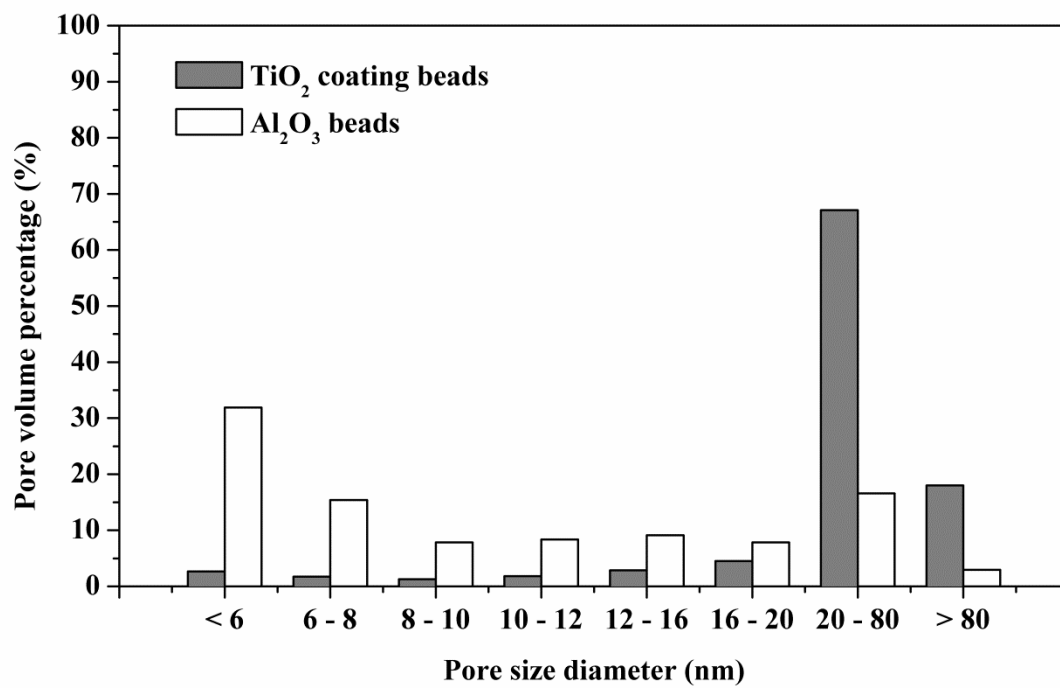
Fig 3.2 Pore size distribution of TiO$_2$-coated beads and Al$_2$O$_3$ beads.
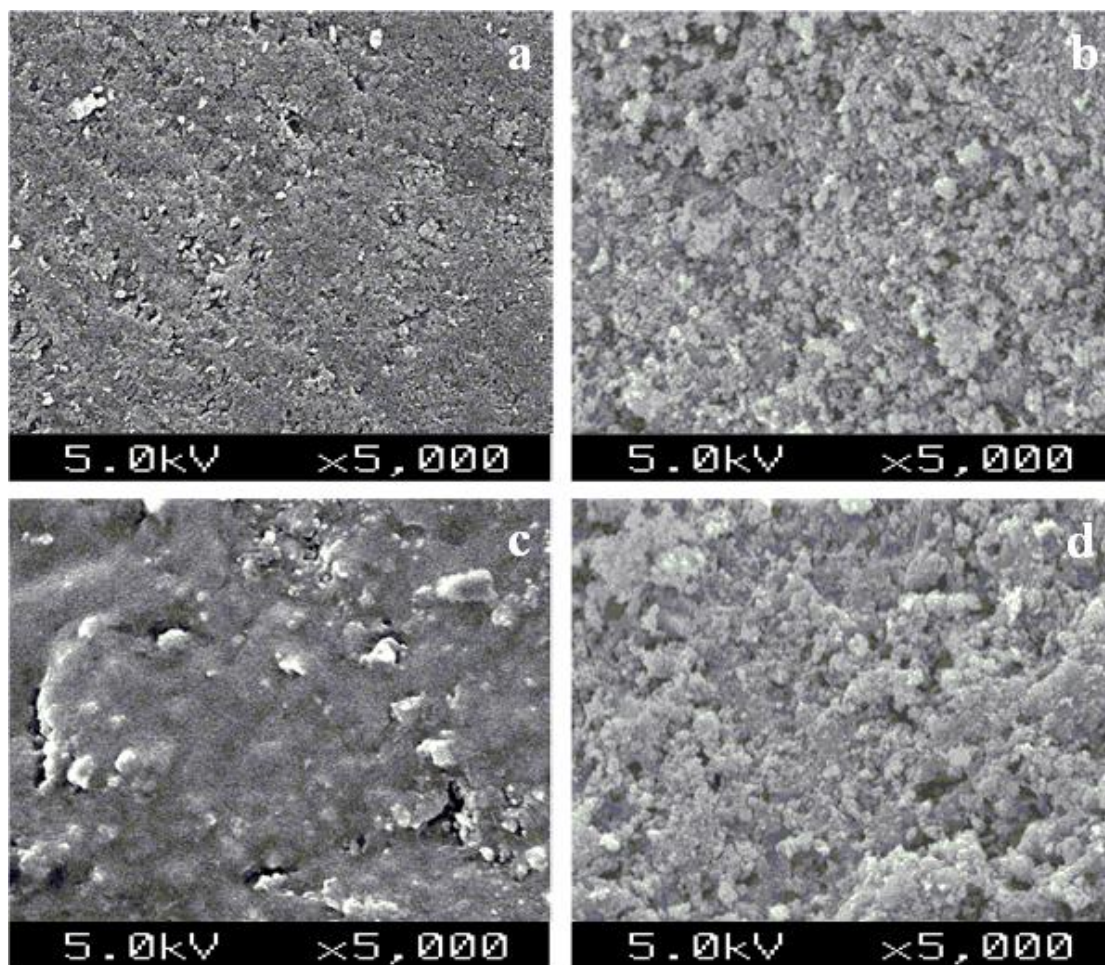
Fig 3.3 SEM images of (a) silica carrier, (b) TiO$_2$-coated beads, (c) Al$_2$O$_3$ beads, and (d) regenerated TiO$_2$-coated beads after five repetitive operations for RhB photocatalytic degradation.
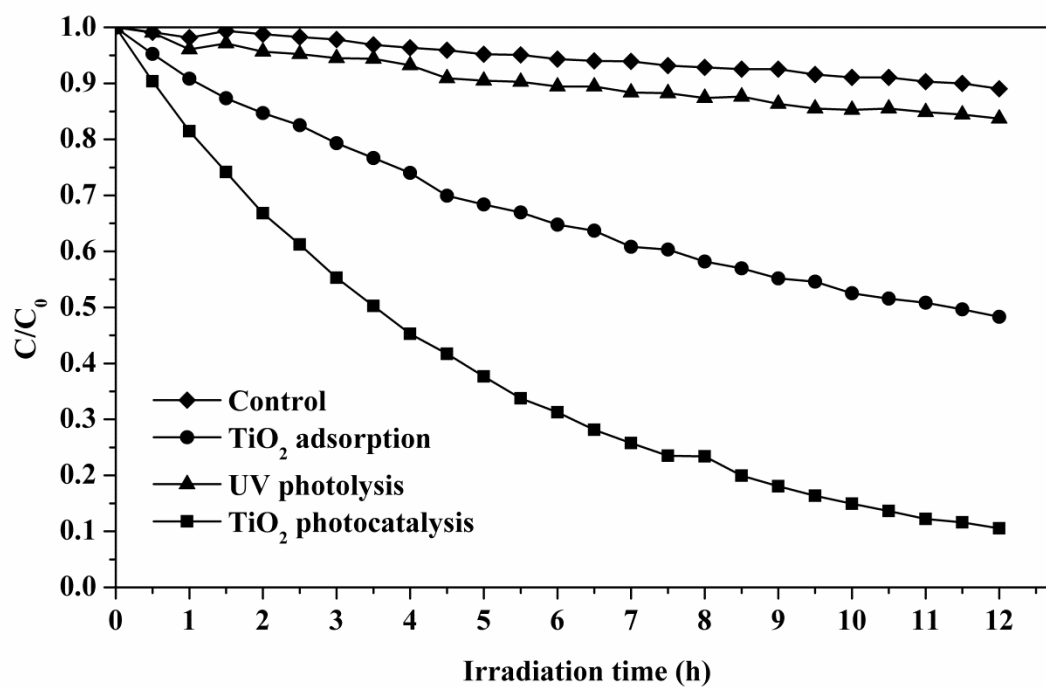
Fig 3.4 RhB removal during 12-h treatment under different conditions.
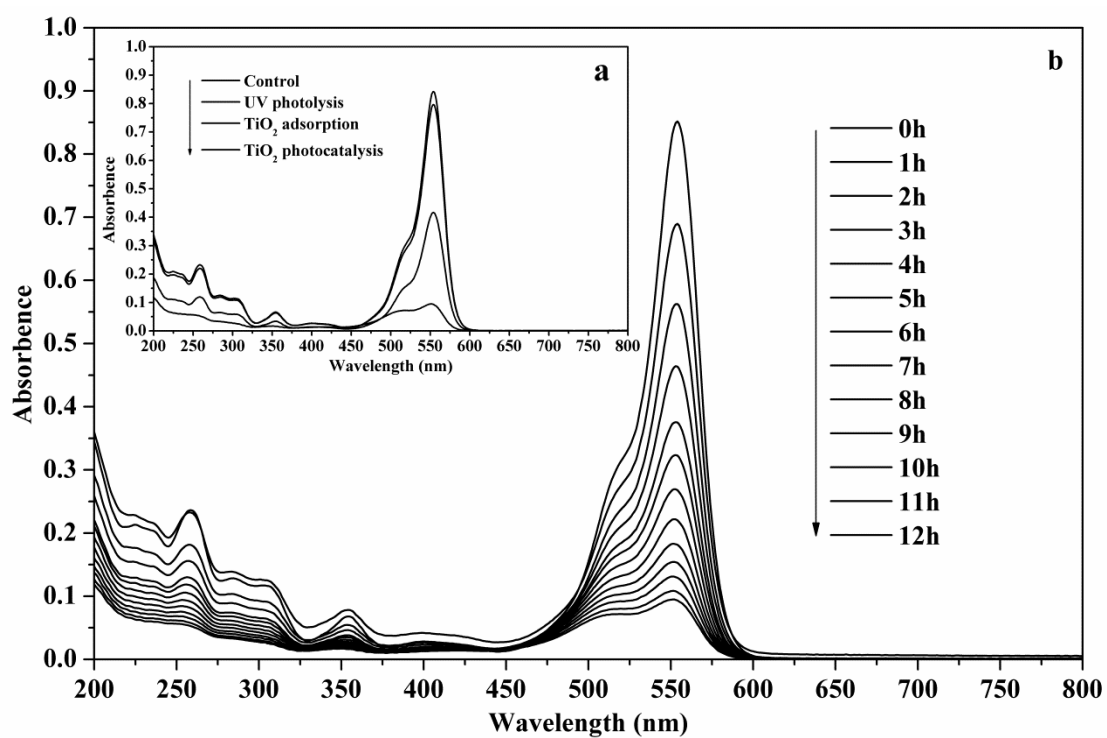
Fig 3.5 UV-VIS-NIR spectral distribution of RhB a) after 12-h treatment of the control, UV photolysis, TiO_2 adsorption and TiO_2 photocatalysis, b) during 12-h TiO_2 photocatalytic degradation.
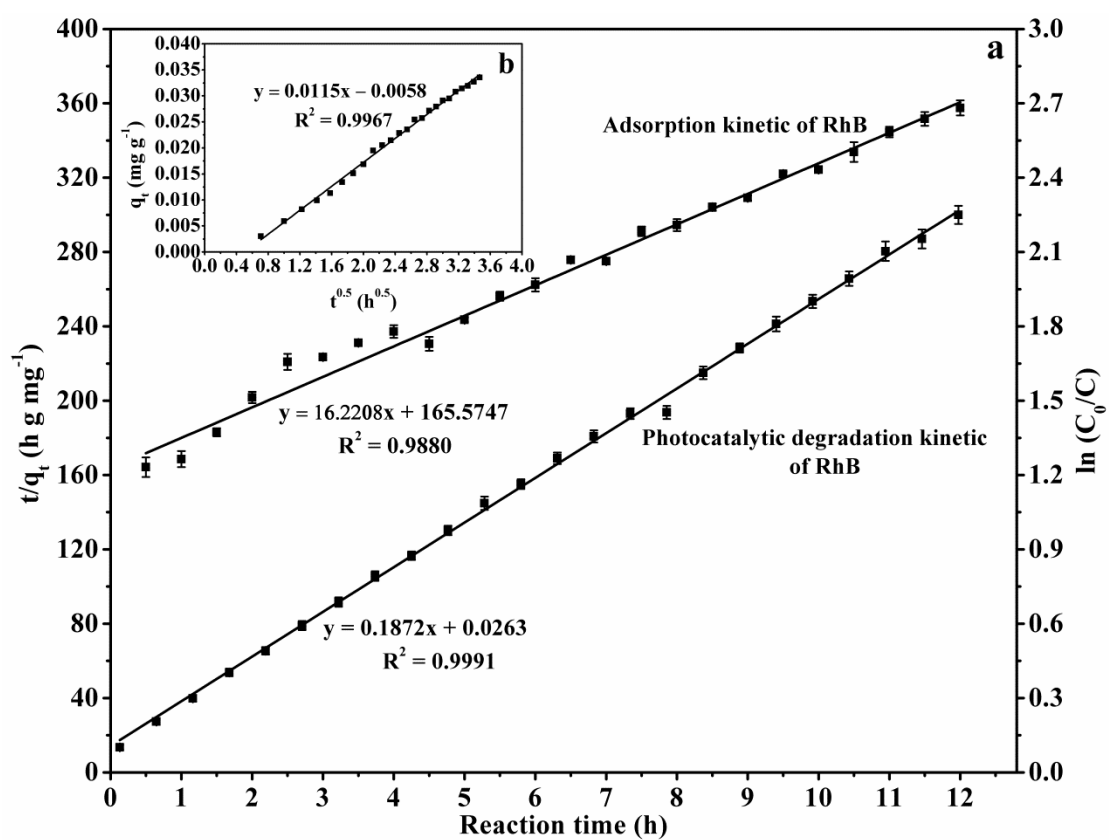
Fig 3.6 Kinetic plots of RhB on TiO$_2$-coated beads a) The adsorption kinetic and photocatalytic degradation kinetic of RhB, b) the intra-particle diffusion kinetic of RhB.
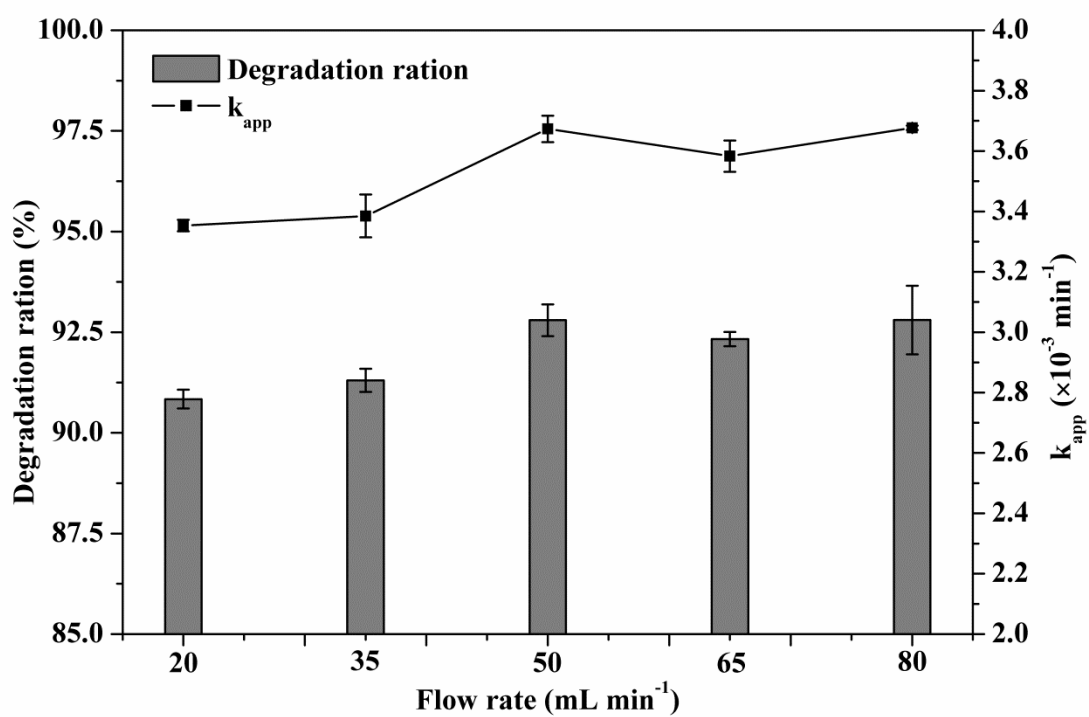
Fig 3.7 Effects of flow rate on the apparent rate constant (k_{app}) and the degradation ration of RhB after 12-h TiO_2 photocatalytic degradation.
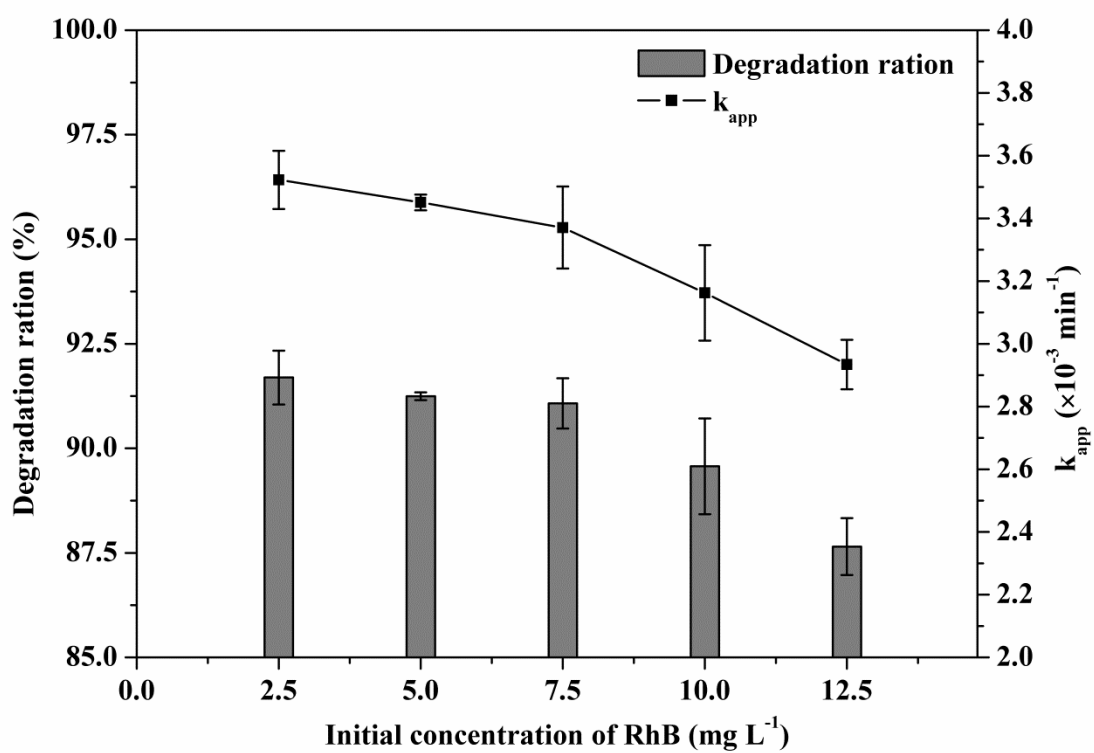
Fig 3.8 Effects of initial concentration on the apparent rate constant (k_{app}) and the degradation ration of RhB after 12-h TiO_2 photocatalytic degradation.
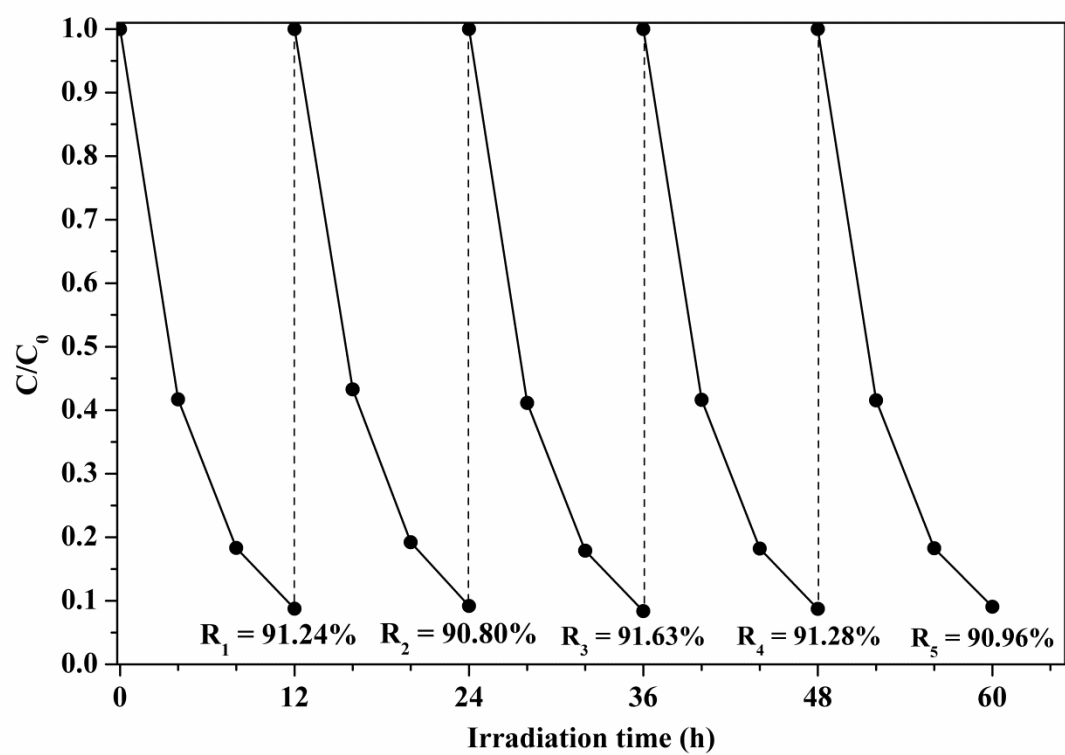
Fig 3.9 Repetitive operation of the developed TiO$_2$-coated beads immobilized photocatalytic reactor (TBIPR) for RhB degradation.

Chapter 4 Pretreatment of high-COD wastewater using developed photocatalytic reactor to improve methane production

4.1 Introduction

Aerobic treatment systems such as the activated sludge process (ASP) are widely used for treating low strength wastewater (< 1000 mg L^{-1} COD) like municipal wastewater. ASP process is energy intensive due to the high aeration requirement. It also produces large quantity of waste activated sludge (WAS) that has to be treated and disposed off. That results in a high operating cost of ASP. Anaerobic treatment of wastewater exhibits cost-efficient even in the case of high COD loading, due to its low sludge production and recovery of bioenergy. However, it has been found to be inefficient for the treatment of high-COD wastewater containing non-biodegradable organic pollutants. In our previous study, a novel TiO$_2$-coated beads immobilized photocatalytic reactor (TBIPR) was developed and successfully applied for the degradation of Rhodamine B and Methyl Orange. In the present study, the developed TBIPR was used for the treatment of high-COD wastewater synthesized using potassium hydrogen phthalate (KHP) as target organic pollutants, and the TiO$_2$ photocatalysis pretreated KHP wastewater was used for methane fermentation.

4.2 Materials and methods

4.2.1 Materials

Potassium hydrogen phthalate (KHP) purchased from Wako Pure Chemical

Industries, Ltd. (Osaka, Japan) was employed to synthesize the high-COD wastewater. Its molecular structure and chemical properties was illustrated in Table 4.1. Before the experiments, wastewaters with COD content of 5000 mg L^{-1} was synthesized using KHP and deionized water. The prepared high-COD wastewaters were stored at $4^{o}C$ in a fridge. The waste activated sludge (WAS) taken from the secondary sedimentation tank of a wastewater treatment plant located in Shimodate (Ibaraki, Japan) was used as the inoculum source. Prior to use, the collected WAS was stored in a refrigerator at $4^{o}C$. Its characteristics were the same as that previously described.

4.2.2 Photocatalytic treatment of high-COD wastewater using developed TBIPR

The prepared 1200 mL of high-COD wastewater was taken in a conical flask (volume capacity: 2000 mL) and passed through the reactor inlet. Then, the synthesized high-COD wastewater was continuously circulated through the reactor and liquid storage tank with magnetic stirring at the flow rate of 50 mL min^{-1} by a recirculation pump, 5 mL of degraded sample was withdrawn every day. The photocatalytic treatment of high-COD wastewater lasted for 30 days. The COD content in all samples were determined using a calibration curve of KHP solution (concentration vs absorbance) prepared separately with known concentration from UV-visible spectra. Absorbance measurement was done using an UV-visible spectrophotometer (UV1800, SHIMADZU, Japan) at 600 nm. Duplicate experiments were conducted under the same condition, and the mean values were used for analyses.

4.2.3 Anaerobic methane fermentation of TiO$_2$ photocatalysis pretreated high-COD wastewater

In this study, the TiO$_2$ photocatalysis pretreated high-COD wastewater synthesized by KHP was used for anaerobic methane fermentation. In order to accelerate the start-up process and achieve a stable anaerobic digestion system, pretreatment of the seed sludge is required to enrich methanogens. A preliminary acclimation of raw WAS was conducted to enrich the methanogens. Firstly, the pH level of raw WAS was adjusted to 7.0 $\pm$ 0.03 by 1 M of NaOH solution. After that, 400 mL WAS was mixed with 0.4 g glucose as the carbon source for bacteria in a 500 mL Schott Duran bottle. Nitrogen gas was injected into the reactor to maintain the anaerobic condition. The acclimation operation was conducted at 35 $\pm$ 1°C for 14 days. The acclimated WAS was used as the inoculum for methane fermentation in this study.

Methane fermentation experiments of TiO$_2$ photocatalysis pretreated high-COD wastewater were performed in batch mode. A number of 50 mL glass test-tubes with sealing caps were used as the bioreactors. Methane fermentation was performed in three groups of bioreactors: (R1) control, 8 mL seeding sludge was mixed with 32 mL deionized water; (R2) KHP wastewater, 8 mL seeding sludge was mixed with 32 mL synthesized high-COD wastewater; and (R3) photocatalysis pretreated KHP wastewater, 8 mL seeding sludge was mixed with 32 mL photocatalysis pretreated KHP wastewater. The initial COD content of R1, R2 and R3 is 3900, 8800 and 9300 mg L^{-1}, respectively. The methane fermentation experiments were carried out at 35 $\pm$

1°C for 30 days. The biogas was collected using a 10 mL plastic syringes, and the volume was read directly using the scale on the syringe. The gas composition was determined by a gas chromatography. Duplicate experiments in each group were carried out under the same condition, and the mean values were used for analysis.

4.2.4 Analytic methods

The pH value was measured using a pH meter (SG8-ELK, SevenGo pro). Total solid content (TS), volatile solid content (VS), chemical oxygen demand (COD) were detected according to the standard methods. The gas composition was detected using a gas chromatography (GC-8A, SHIMADZU, Japan) equipped with a thermal conductivity detector and a Porpapak Q column.

4.3 Results and discussion

4.3.1 Photocatalytic pretreatment of high-COD wastewater using developed TBIPR

The developed TBIPR was used to treat synthesized high-COD wastewater by a series of continuous experiments. As shown in Fig. 4.1, the pH value of the synthesized wastewater increased with the irradiation time. After 30-d photocatalytic treatment, the pH value increased to 5.25 from initial 4.05. This result can be ascribed to the broken up of carboxyl groups (-COOH) in the KHP molecules during its photocatalytic degradation.

Fig. 4.2 illustrates the variation of COD content and COD removal ratio during 30-d photocatalytic treatment of the synthesized high-COD wastewater. After 30-d

photocatalytic degradation, the COD content of synthesized wastewater decreased from 5000 to 2137 mg L^{-1}. The corresponding COD removal ratio by the photocatalytic treatment using developed TBIPR reached 57.26%. The developed TBIPR exhibited excellent performance for the treatment of synthesized high-COD wastewater containing non-biodegradable KHP.

4.3.2 Anaerobic methane fermentation of TiO_2 photocatalysis pretreated high-COD wastewater

Fig. 4.3 shows the cumulative methane production of the control (R1), KHP wastewater (R2) and TiO_2 photocatalysis pretreated KHP wastewater (R3). Both the bioreactors R1 and R2 required 4-d start-up period for methane production. While that of bioreactor R3 is just 2 days, indicating that TiO_2 photocatalytic pretreatment enhanced the biodegradability of KHP thereby shortened the start-up period of consequent methane fermentation process. After 14-d anaerobic fermentation, the methane production of R1, R2 and R3 bioreactors was 6.99, 6.50 and 146.70 mL-CH_4/g-COD, respectively. The methane production of control bioreactor mainly derived from the bioconversion of organic compounds in the seeing sludge. The methane production of bioreactor R2 was slightly lower than that of the control one due to its higher COD loading which inhibited the activity of methanogens. The bioreactor R3 obtained the highest methane production in comparison with R2 and the control. This result showed that TiO_2 photocatalytic pretreatment of high-COD wastewater using developed TBIPR obviously improved the methane production in the consequent anaerobic fermentation.

4.4 Summary

In the present study, the developed TBIPR was used for the treatment of high-COD wastewater synthesized using potassium hydrogen phthalate (KHP) as target organic pollutants, then the TiO_2 photocatalysis pretreated KHP wastewater was used for methane fermentation. After 30-d photocatalytic treatment, the pH value increased to 5.25 from initial 4.05. This result can be ascribed to the broken up of carboxyl groups (-COOH) in the KHP molecules during its photocatalytic degradation. The corresponding COD removal ratio by the photocatalytic treatment using developed TBIPR reached 57.3%. The developed TBIPR exhibited excellent performance for the treatment of synth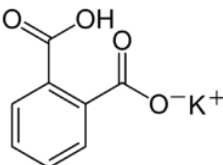esized high-COD wastewater containing non-biodegradable KHP. Then, after 14-d mesophilic anaerobic fermentation, the methane production from TiO_2 photocatalysis pretreated KHP wastewater reached 146.70 mL-CH_4/g-COD, which was much higher than that of the control (6.99 mL-CH_4/g-COD). This result showed that TiO_2 photocatalytic pretreatment of high-COD wastewater using developed TBIPR obviously improved the methane production in the consequent anaerobic fermentation.

Table 4.1 Molecular structure and chemical properties of potassium hydrogen phthalate (KHP).

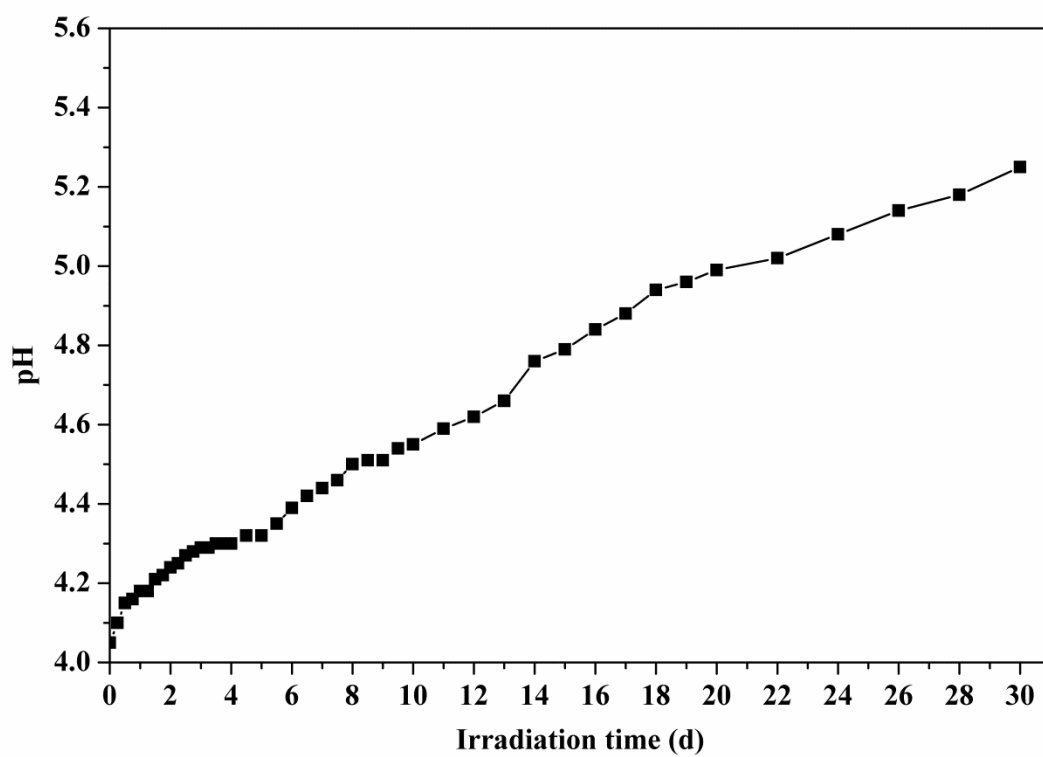| Molecular structure	Chemical properties	
potassium hydrogen phthalate (KHP)		
	Chemical formula	$KHC_8H_4O_4$
	Molecular weight	204.22 g mol^{-1}
	Density	1.64 g cm^{-3}
	Class	Aromatic acid salt

Fig 4.1 The pH variation in photocatalytic degradation of KHP using developed TBIPR.
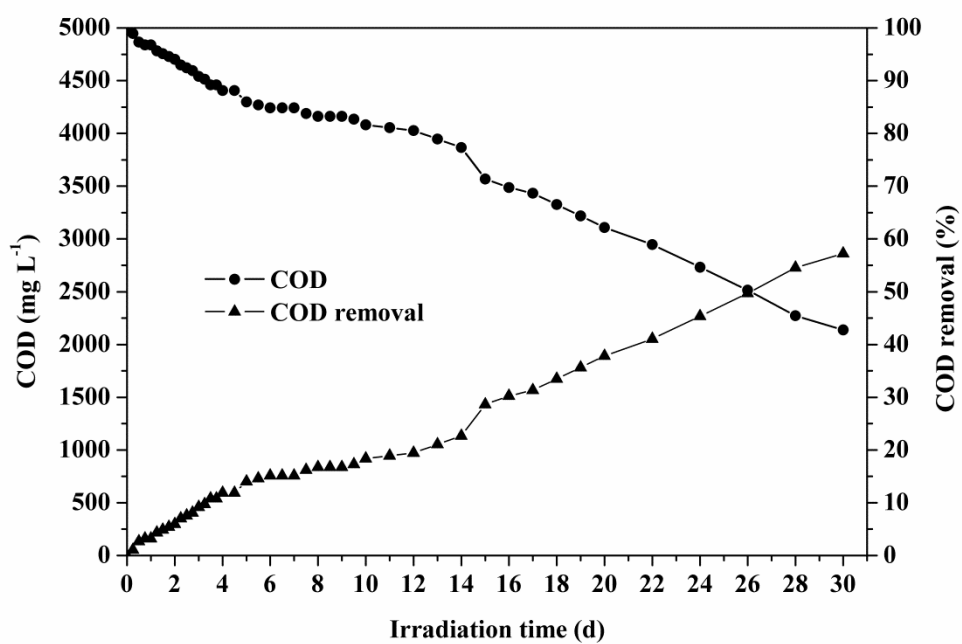
Fig 4.2 The time course of COD content and COD removal ratio in photocatalytic degradation of KHP using developed TBIPR.
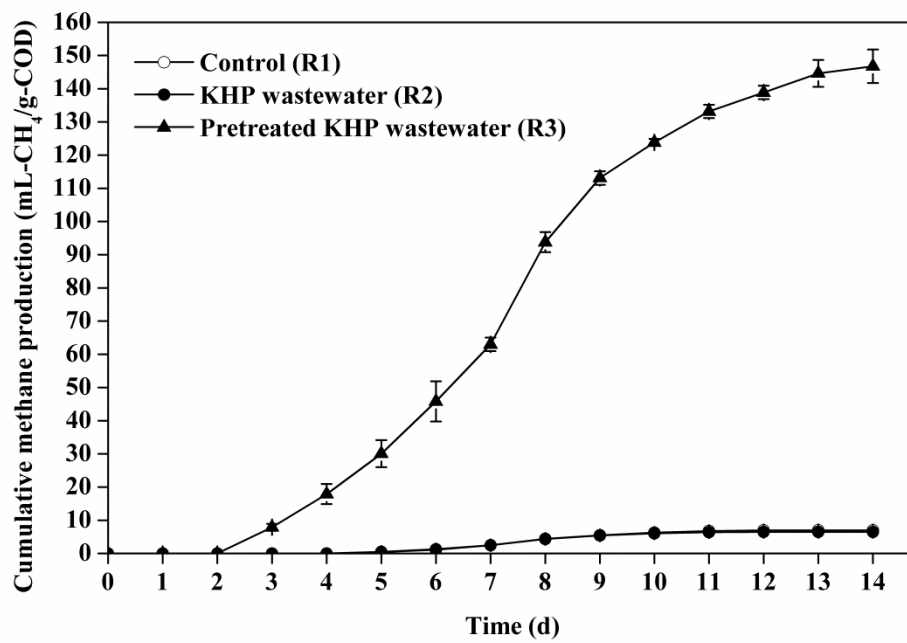
Fig 4.3 The cumulative methane production from TiO$_2$ photocatalysis pretreated high-COD wastewater synthesized using KHP as model organic pollutant.

Chapter 5 Conclusions

5.1 Using TiO$_2$ photocatalysis as a pretreatment of waste activated sludge to enhance the biohydrogen production

The effects of TiO$_2$ photocatalysis on the hydrolysis of protein of waste activated sludge and its biodegradability were investigated. It can be concluded from the results that:

(1) TiO$_2$ photocatalysis improved the nonenzymatic degradation of protein to carboxylic acids and ammonia. The optimal condition for photocatalytic degradation of protein is TiO$_2$ dosage of 5.0 mg L^{-1} under 2.4 w m^{-2} UV light irradiation.

(2) The hydrogen production from TiO$_2$ photocatalysis pretreated WAS after 96-h mesophilic fermentation reached 11.7 mL-H$_2$/g-VS, which was approximately 2.2 times of that from the control.

(3) TiO$_2$ photocatalytic pretreatment of WAS obviously accelerated the hydrolysis of its macromolecular components like protein and improved the hydrogen production in the subsequent biohydrogen fermentation.

5.2 Development of TiO$_2$-coated beads immobilized photocatalytic reactor for decomposing recalcitrant organic pollutants

A novel TiO$_2$-coated beads immobilized photocatalytic reactor (TBIPR) was developed and successfully applied for the degradation of Rhodamine B and Methyl Orange. The conclusions were draw as follows:

(1) The high adsorption capacity of TiO$_2$-coated beads facilitates the photocatalytic

degradation of target organics by improving the transportation of organic molecules to the vicinity of photocatalytic sites.

(2) Flow rate affects the photocatalytic reaction mainly by changing the convective mass transfer and contact time of dye molecules with TiO_2 surface in the developed TBIPR. There exists an optimal flow rate for the photocatalytic degradation of target organics using developed TBIPR.

(3) The developed TBIPR exhibits high efficiency, low-energy consumption and excellent repetitive operation performance. It is a promising alternative for the decomposition of recalcitrant organic contaminants in wastewater using developed TBIPR.

5.3 Pretreatment of high-COD wastewater using developed photocatalytic reactor to improve methane production

In the present study, the developed TBIPR was used for the treatment of high-COD wastewater synthesized using potassium hydrogen phthalate (KHP) as target organic pollutant, then the TiO_2 photocatalysis pretreated KHP wastewater was used for methane fermentation. Following conclusions were obtained via discussing the experimental results.

(1) After 30-d photocatalytic treatment, the pH value increased to 5.25 from initial 4.05. This result can be ascribed to the broken up of carboxyl groups (-COOH) in the KHP molecules during its photocatalytic degradation.

(2) The corresponding COD removal ratio by the photocatalytic treatment using developed TBIPR reached 57.3%. The developed TBIPR exhibited excellent

performance for the treatment of synthesized high-COD wastewater containing non-biodegradable KHP.

(3) After 14-d mesophilic anaerobic fermentation, the methane production from TiO_2 photocatalysis pretreated KHP wastewater reached 146.70 mL-CH_4/g-COD, which was much higher than that of the control (6.99 mL-CH_4/g-COD). This result showed that TiO_2 photocatalytic pretreatment of high-COD wastewater using developed TBIPR obviously improved the methane production in the consequent anaerobic fermentation.

5.4 Future research

In this study, a novel TiO_2-coated beads immobilized photocatalytic reactor (TBIPR) was developed and successfully applied for the degradation of Rhodamine B and Methyl Orange. The developed TBIPR exhibited great potentiality for the decomposition of recalcitrant organic contaminants in wastewater. For the practical application of this photocatalytic reactor, many issues should be further investigated in the future research that is listed as follows:

(1) Using developed TBIPR for the photocatalytic pretreatment of WAS to enhance the fermentative biogas production.

(2) Synthesizing immobilized visible-light-sensitive photocatalysts to substitute the TiO_2-coated beads in developed TBIPR for utilizing solar light as the irradiation source.

References

[1] L. Appels, J. Baeyens, J. Degreve, R. Dewil, Principles and potential of the anaerobic digestion o waste-activated sludge, Progress in Energy and Combustion Science, 34 (2008) 755-781.

[2] J. Laurent, M. Casellas, H. Carrère, C. Dagot, Effects of thermal hydrolysis on activated sludge solubilization, surface properties and heavy metals biosorption, Chemical Engineering Journal, 166 (2011) 841-849.

[3] Y. S. Sohn, Y. R. Smith, M. Misra, V. Subramanian, Electrochemically assisted photocatalytic degradation of methyl organge using anodized titamium dioxide nanotubes, Applied Catalysis B: Environmental, 84 (2008) 372-378.

[4] B. Damardji, H. Khalaf, L. Duclaux, B. David, Preparation of TiO_2-pillared montmorillonite as photocatalyst Part II Photocatalytic degradation of a textile azo dye, Applied Clay Science, 45 (2009) 98-104.

[5] A. Veeken, B. Hamelers, Effect of substrate-seed mixing and leachate recirculation on solid state digestion of biowaste, Water Science and Technology, 41 (2000) 255-262.

[6] W. B. Whitman, et al., The methanogenic bacteria, Prokaryotes, 3 (2006) 165-207.

[7] D. Traversi, S. Villa, L. Eugenio, R. Degan, G. Gilli, Application of a real-qPCR method to measure the methanogen concentration during anaerobic digestion as an indicator of biogas production capacity, Journal of Environmental Management, 111 (2012) 173-177.

[8] D. W. Li, T. Zhou, L. Chen, W. Z. Jiang, F. Cheng, B. M. Li, Y. Kitamura, Using porphyritic andesite as a new additive for improving hydrolysis and acigogennesis of solid organic wastes, Bioresource Technology, 100 (2009) 5594-5599.

[9] V. A. Vavilin, B. Fernandez, J. Palatsi, X. Flotats, Hydrolysis kinetics in anaerobic degradation of particulate organic material: an overview, Waste Management, 28 (2008) 939-951.

[10] F. Cheng, M. Li, D. W. Li, L. Chen, W. Z. Jiang, Y. Kitamura, B. M. Li, Volatile organic acid adsorption and cation dissociation by porphyritic andesite for enhancing hydrolysis an acidogenesis of solid food wastes, Biresource Technology, 101 (2010) 5076-5083.

[11] M. Climent, I. Ferrer, M. M. Baeza, A. Artola, F. Vázquez, X. Font, Effects of thermal and mechanical pretreatment of secondary sludge on biogas production under thermophilic conditions, Chemical Engineering Journal, 133 (2007) 335-342.

[12] A. Donoso-Bravo, S. Pérez-Elvira, E. Aymerich, F. Fdz-Polanco, Assessment of the influence of thermal pre-treatment time on the macromolecular composition and anaerobic biodegradability of sewage sludge, Bioresource Technology, 102 (2011) 660-666.

[13] E. Neyens, J. Baeyens, M. Weemaes, B. De heyder, Hot acid hydrolysis as a potential treatment of thickened sewage sludge, Journal of Hazardous Materials, 98 (2003) 275-293.

[14] D. H. Kim, E. Jeong, S. E. Oh, H. S. Shin, Combined (alkaline + ultrasonic) pretreatment effect on sewage sludge disintegration, Water Research, 44 (2010)

3093-3100.

[15] Y. Y. Yan, L. Y. Feng, C. J. Zhang, C. Wisniewski, Q. Zhou, Ultrasonic enhancement of waste activated sludge hydrolysis and volatile fatty acids accumulation at pH 10.0, Water Research, 44 (2010) 3329-3336.

[16] G. M. Zhang, J. Yang, H. Z. Liu, J. Zhang, Sludge ozonation: Disintegration, supernatant changes and mechanisms, Bioresource Technology, 100 (2009) 1505-1509.

[17] G. H. Xu, S. H. Chen, J. W. Shi, S. M. Wang, C. F. Zhu, Combination treatment of ultrasound and ozone for improving solubilization and anaerobic biodegradability of waste activated sludge, Journal of Hazardous Materials, 180(2010) 340-346.

[18] D. Ljubas, Solar photocatalysis–a possible step in drinking water treatment, Energy, 30 (2005) 1699-1710.

[19] T. Van Gerven, G. Mul, J. Moulijin, A. Stankiewicz, A review of intensification of photocatalytic processes, Chemical Engineering and Processing: Process Intensification, 46 (2007) 781-789.

[20] J. Shang, Y. C. Zhang, T. Zhu, Q. Wang, H. Song, The promoted photoelectrocatalytic degradation of rhodamine B over TiO2 thin film under the half-wave pulsed direct current, Applied Catalysis B: Environmental, 102 (2011) 464-469.

[21] R. A. Damodar, S. J. You, S. H. Ou, Coupling of membrane separation with photocatalytic slurry reactor for advanced dye wastewater treatment, Separation and Purification Technology, 76 (2010) 64-71.

[22] S. Mozia, Photocatalytic membrane reactor (PMRs) in water and wastewater treatment. A review, Separation and Purification Technology, 73 (2010) 71-91.

[23] R. A. Damodar, S. J. You, G. W. Chiou, Investigation on the conditions mitigating membrane fouling caused by TiO_2 deposition in a membrane photocatalytic reactor (MPR) used for dye wastewater treatment, Journal of Hazardous Materials, 203-204 (2012) 348-356.

[24] M. R. Hoffmann, S. T. Martin, W. Choi, D. W. Bahnemann, Environmental application of semiconductor photocatalysis, Chemical Reviews, 95 (1995) 69-96.

[25] S. P. Kamble, S. B. Sawant, V. G. Pangarkar, Batch and continuous photocatalytic degradation of benzenesulfonic acid using concentrated solar radiation, Indurial & Engineering Chemistry Research, 42 (2003) 6705-6713.

[26] S. Kaneco, M. Arifur Rahmana, T. Suzuki, H. Katsumata, K. Ohta, Optimization of solar photocatalytic degradation conditions of bisphenol A in water using titanium dioxide, Journal of Photochemistry and Photobiology A: Chemisty, 163 (2004) 419-424.

[27] I. K. Konstantinou, T. A. Albanis, TiO_2-assisted photocatalytic degradation of azo dyes in acqueous solution: kinetic and mechanistic investigations: A review, Applied catalysis B: Environmental, 49 (2004) 1-14.

[28] Y. Paz, Preferential Photodegradation-Why and How?, Comptes Rendus Chimie, 9 (2006) 774-787.

[29] D. F. Ollis, E. Pelizzetti, N. Serpone, Photocatalyzed destruction of water contaminants, Environmental Science & Technology, 25 (1991) 1522-1529.

[30] T. E. Doll, F. H. Frimmel, Cross-flow microfiltration with periodical back-washing for photocatalytic degradation of pharmaceutical and diagnostic residues-evaluation of the long-term stability of the photocatalytic activity of TiO_2, Water Research, 39 (2005) 847-854.

[31] H. Y. Chen, O. Zahraa, M. Bouchy, Inhibition by inorganic ions of the adsorption and the photocatalytic degradation of organic contaminants in TiO_2 aqueous suspension, Journal of photochemistry and Photobiology A: Chemistry, 108 (1997) 37-44.

 [32] J. L. Campos, L. Otero, A. Franco, A. Mosquera-Corral and E. Roca, Ozonation strategies to reduce sludge production of a seafood industry WWTP, Bioresource Technology, 100 (2009) 1069-1073.

[33] C. H. Ting and D. J. Lee, Production of hydrogen and methane from wastewater sludge using anaerobic fermentation, International Journal of Hydrogen Energy, 32 (2007) 677-682.

[34] E. Athanasoulia, P. Melidis and A. Aivasidis, Optimization of biogas production of waste activated sludge through serial digestion, Renewable Energy, 47 (2012) 147-151.

[35] F. Morgan-Sagastume, S. Pratt, A. Karlsson, D. Cirne, P. Lant and A. Werker, Production of volatile fatty acids by fermentation of waste activated sludge pre-treated in full-scale thermal hydrolysis plants, Bioresource Technology, 102 (2011) 3089-3097.

[36] J. Clemens, M. Trimborn, P. Weiland and B. Amon, Mitigation of greenhouse

gas emissions by anaerobic digestion of cattle slurry, Agriculture, Ecosystems Environment, 112 (2006) 171-177.

[37] P. Kampas, S. A. Parsons, P. Pearce, S. Ledoux, P. Vale, J. Churchley and E. Cartmell, Mechanical sludge disintegration for the production of carbon source for biological nutrient removal, Water Research, 41 (2007) 1734-1742.

[38] J. Laurent, M. Casellas, H. Carrere and C. Dagot, Effects of thermal hydrolysis on activated sludge solubilization, surface properties and heavy metals biosorption, Chemical Engineering Journal, 166 (2011) 841-849.

[39] H. Carrere, Y. Rafrafi, A. Battimelli, M. Torrijos, J. P. Delgenes and C. Motte, Improving methane production during the codigestion of waste-activated sludge and fatty wastewater: Impact of thermo-alkaline pretreatment on batch and semi-continuous process, Chemical Engineering Journal, 210 (2012) 404-409.

[40] D. C. Devlin, S. R. R. Esteves, R. M. Dinsdale and A. J. Guwy, The effect of acid pretreatment on the anaerobic digestion and dewatering of waste activated sludge, Bioresource Technology, 102 (2011) 4076-4082.

[41] Y. Z. Chi, Y. Y. Li, X. N. Fei, S. P. Wang, H. Y. Yuan, Enhancement of thermophilic anaerobic digestion of thickened waste activated sludge by combined microwave and alkaline pretreatment, Journal of Environmental Sciences, 23 (2011) 1257-1265.

[42] H. C. Xu, P. J. He, G. H. Yu and L. M. Shao, Effect of ultrasonic pretreatment on anaerobic digestion and its sludge dewaterability, Journal of Environmental Sciences, 23 (2011) 1472-1478.

[43] S. Sahinkaya and M. F. Sevimli, Synergistic effects of sono-alkaline pretreatment on anaerobic biodegradability of waste activated sludge, Journal of Industrial and Engineering Chemistry, 19 (2013) 197-206.

[44] S. S. Yang, W. Q. Guo, G. L. Cao, H. S. Zheng and N. Q. Ren, Simultaneous waste activated sludge disintegration and biological hydrogen production using an ozone/ultrasound pretreatment, Bioresource Technology, 124 (2012) 347-354.

[45] Y. Yu, W. I. Chan, P. H. Liao and K. V. Lo, Disinfection and solubilization of sewage sludge using the microwave enhanced advanced oxidation process, Journal of Hazardous Material, 181 (2010) 1143-1147.

[46] L. Appels, A. V. Assche, K. Willems, J. Degreve, J. V. Impe and R. Dewil, Peracetic acid oxidation as an alternative pre-treatment for the anaerobic digestion of waste activated sludge, Bioresource Technology, 102 (2011) 4124-4130.

[47] D. Friedmann, C. Mendive and D. Bahnemann, TiO_2 for water treatment: Parameters affecting the kinetics and mechanisms of photocatalysis, Applied Catalysis B: Environment, 99 (2010) 398-406.

[48] R. Poblete, E. Otal, L. F. Vilches, J. Vale and C. Fernandez-Pereira, Photocatalytic degradation of humic acids and landfill leachate using a solid industrial by-products containing TiO_2 and Fe, Applied Catalysis B: Environment, 102 (2011) 172-179.

[49] A. Fujishima, X. T. Zhang and D. Tryk, TiO_2 photocatalysis and related surface phenomena, Surface Science Report, 63 (2008) 515-582.

[50] S. H. Wang and S. Q. Zhou, Photodegradation of methyl orange by

photocatalyst of CNTs/P-TiO$_2$ under UV and visible-light irradiation, Journal of Hazardous Material, 185 (2011) 77-85.

[51] C. S. Guo, J. Xu, Y. He, Y. Zhang, Y. Q. Wang, Photodegradation of rhodamine B and methyl orange over one-dimensional TiO$_2$ catalysts under simulated solar irradiation, Applied Surface Science, 257 (2011) 3798-3803.

[52] J. A. Rengifo-Herrera, M. N. Blanco and L. R. Pizzio, Photocatalytic bleaching of aqueous malachite green solutions by UV-A and blue-light-illuminated TiO$_2$ spherical nanoparticles modified with tungstophosphoric acid, Applied Catalysis B: Environment, 110 (2011) 126-132.

[53] G. Xue, H. H. Liu, Q. Y. Chen, C. Hills, M. Tyrer, F. Innocent, Synergy between surface adsorption and photocatalysis during degradation of humic acid on TiO$_2$/activated carbon composites, Journal of Hazardous Material, 186 (2011) 765-772.

[54] M. H. Ahmed, T. E. Keyes, J. A. Byrne, C. W. Blackledge and J. W. Hamilton, Adsorption and photocatalytic degradation of human serum albumin on TiO$_2$ and Ag-TiO$_2$ films, Journal of Photochemistry and Photobiology A: Chemistry, 222 (2011) 123-131.

[55] S. Chang, J. Z. Li and F. Liu, Evaluation of different pretreatment methods for preparing hydrogen-producing seed inocula from waste activated sludge, Renewable Energy, 36 (2011) 1517-1522.

[56] M. M. Bradford, A rapid and sensitive method for the quantitation of microgram quantities of protein utilizing the principle or protein-dye binding, Analytical

Biochemistry, 72 (1976) 248-254.

[57] A. D. Eaton, L. S. Clesceri, E. W. Rice, A. E. Greenberg, Standard methods for the examination of water and wastewater, American Public Health Association (APHA), 5220D (20055) 5-18～5-19.

[58] K. V. Kumar, K. Porkodi, F. Rocha, Langmuir-Hinshelwood kinetics − A theoretical study, Catalysis Communication, 9 (2008) 82-84.

[59] B. Neppolian, H. C. Choi, S. Sakthivel, B. Arabindoo, V. Murugesan, Solar light induced TiO_2 assisted degradation of textile dye reactive blue 4, Chemosphere, 46 (2002) 1173-1181.

[60] K. Natarajan, T. S. Natarajan, H. C. Bajaj, R. J. Tayade, Photocatalytic reactor based on UV-LED/TiO_2 coated quartz tube for degradation of dyes, Chemical Engineering Journal, 178 (2011) 40-49.

[61] A. Akyol, M. Bayramoglu, The degradation of an azo dye in a batch slurry photocatalytic reactor, Chemical Engineering Processing, 47 (2008) 2150-2156.

[62] K. P. Mishra, P. R. Gogate, Intensification of degradation of aqueous solutions of rhodamine B using sonochemical reactors at operating capacity of 7 L, Journal Environmental Management, 92 (2011) 1972-1977.

[63] R. V. Grieken, J. Marugán, C. Sordo, C. Pablos, Comparison of the photocatalytic disinfection of E. coli suspensions in slurry, wall and fixed-bed reactors, Catalysis Today, 144 (2009) 48-54.

[64] D. Friedmann, C. Mendive, D. Bahnemann, TiO_2 for water treatment: Parameters affecting the kinetics and mechanisms of photocatalysis, Applied

Catalysis B: Environmental, 99 (2010) 398-406.

[65] S. Krejčíková, L. Matějová, K. Kočí, L. Obalová, Z. Matěj, L. Čapek, O. Šolcová, Preparation and characterization of Ag-doped crystalline titania for photocatalysis applications, Applied Catalysis B: Environmental, 111-112 (2012) 119-125.

[66] S. H. Wang, S. Q. Zhou, Photodegradation of methyl orange by photocatalyst of CNTs/P-TiO_2 under UV and visible-light irradiation, Journal of Hazardous Materials, 185 (2011) 77-85.

[67] C. S. Guo, J. Xu, Y. He, Y. Zhang, Y. Q. Wang, Photodegradation of rhodamine B and methyl orange over one-dimensional TiO_2 catalysts under simulated solar irradiation, Applied Surface Science, 257 (2011) 3798-3803.

[68] J. A. Rengifo-Herrera, M. N. Blanco, L. R. Pizzio, Photocatalytic bleaching of aqueous malachite green solutions by UV-A and blue-light-illuminated TiO_2 spherical nanoparticles modified with tungstophosphoric acid, Applied Catalysis B: Environmental, 110 (2011) 126-132.

[69] G. Xue, H. H. Liu, Q. Y. Chen, C. Hills, M. Tyrer, F. Innocent, Synergy between surface adsorption and photocatalysis during degradation of humic acid on TiO_2/activated carbon composites, Journal of Hazardous Materials, 186 (2011) 765-772.

[70] Y. Yao, K. Li, S. Chen, J. P. Jia, Y. L. Wang, H. W. Wang, Decolorization of Rhodamine B in a thin-film photoelectrocatalytic (PEC) reactor with slant-placed TiO_2 nanotubes electrode, Chemical Engineering Journal, 187 (2012) 29-35.

[71] A. Y. Zhang, M. H. Zhou, L. Han, Q. X. Zhou, The combination of rotating disk photocatalytic reactor and TiO_2 nanotube arrays for environmental pollutants removal, Journal of Hazardous Materials, 186 (2011) 1374-1383.

[72] L. L. P. Lim, R. J. Lynch, A proposed photocatalytic reactor design for in situ groundwater applications, Applied Catalysis A: General, 378 (2010) 202-210.

[73] P. Du, J. T. Carneiro, J. A. Moulijn, G. Mul, A novel photocatalytic monolith reactor for multiphase heterogeneous photocatalysis, Applied Catalysis A: General, 334 (2008) 119-128.

[74] M. H. Li, K. J. Czymmek, C. P. Huang, Responses of Ceriodaphnia dubia to TiO_2 and Al_2O_3 nanoparticles: A dynamic nano-toxicity assessment of energy budget distribution, Journal of Hazardous Materials, 187 (2011) 502-508.

[75] D. Zheng, N. Wang, X. M. Wang, Y. Tang, L. H. Zhu, Z. Huang, H. Q. Tang, Y. Shi, Y. T. Wu, M. Zhang, B. Lu, Effects of the interaction of TiO_2 nanoparticles with bisphenol A on their physicochemical properties and in vitro toxicity, Journal of Hazardous Materials, 199-200 (2012) 426-432.

[76] C. Shen, Y. J. Wang, J. H. Xu, G. S. Luo, Facile synthesis and photocatalytic properties of TiO_2 nanoparticles supported on porous glass beads, Chemical Engineering Journal, 209 (2012) 478-485.

[77] M. Q. Wang, J. Yan, H. P. Cui, S. G. Du, Low temperature preparation an characterization of TiO_2 nanoparticles coated glass beads by heterogeneous nucleation method, Materials Characterization, 2013 (2013) 39-47.

[78] M. H. Ahmed, T. E. Keyes, J. A. Byrne, C. W. Blackledge, J. W. Hamilton,

Adsorption and photocatalytic degradation of human serum albumin on TiO_2 and Ag-TiO_2 films, Journal of Photochemistry and Photobiology A: Chemistry, 222 (2011) 123-131.

[79] V. G. Milt, S. Ivanova, O. Sanz, M. I. Domínguez, A. Corrales, J. A. Odriozola, M. A. Centeno, Au/TiO_2 supported on ferritic stainless steel monoliths as CO oxidation, Applied Surface Science, 2010 (2013), doi: 10.1016/j.apsusc. 2012.12.159.

[80] X. D. Wang, F. Shi, W. Huang, C. M. Fan, Synthesis of high quality TiO_2 membranes on alumina supports and their photocatalytic activity, Thin Solid Films, 520 (2012) 2488-2492.

[81] Y. J. Li, X. M. Zhou, W. Chen, L. Y. Li, M. X. Zen, S. D. Qin, S. G. Sun, Photodecolorization of Rhodamine B on tungsten-doped TiO_2/activated carbon under visible-light irradiation, Journal of Hazardous Materials, 227-228 (2012) 25-33.

[82] M. H. Baek, J. W. Yoon, J. S. Hong, J. K. Suh, Application of TiO_2-containing mesoporous spherical activated carbon in a fluidized bed photoreactor-Adsorption and photocatalytic activity, Applied Catalysis A: General, 450 (2013) 222-229.

[83] M. Khatamian, S. Hashemian, A. Yavari, M. Saket, Preparation of metal ion (Fe^{3+} and Ni^{2+}) doped TiO_2 nanoparticles supported on ZSM-5 zeolite and investigation of its photocatalytic activity, Materials Science and Engineering B, 177 (2012) 1623-1627.

[84] T. Kamegawa, R. Kido, D. Yamahana, H. Yamashita, Design of TiO_2-zeolite composites with enhanced photocatalytic performances under irradiation of UV and

visible light, Microporous and Mesoporous Materials, 165 (2013) 142-147.

[85] S. R. Patil, B. H. Hameed, A. S. Škapin, U. L. Štangar, Alternate coating and porosity as dependent factors for the photocatalytic activity of sol-gel derived TiO_2 films, Chemical Engineering Journal, 174 (2011) 190-198.

[86] J. B. Naceur, M. Gaidi, F. Bousbih, R. Mechiakh, R. Chtourou, Annealing effects on microstructural and optical properties of Nanostructured-TiO_2 thin films prepared by sol-gel technique, Current Applied Physics, 12 (2012) 22-428.

[87] M. C. Gil, I. V. Driessche, S. V. Gils, P. Lommens, P. Cas telein, High-throughput analysis for preparation, processing and analysis of TiO_2 coating on steel by chemical solution deposition, Journal of Alloys and Compounds, 540 (2012) 170-178.

[88] M. Y. Song, Y. K. Park, J. S. Jurng, Direct coating of V_2O_5/TiO_2 nanoparticles onto glass beads by chemical vapor deposition, Powder Technology, 231 (2012) 135-140.

[89] R. C. Adochite, D. Munteanu, M. Torrell, L. Cunha, E. Alves, N. P. Barradas, A. Cavaleiro, J. P. Riviere, E. Le Bourhis, D. Eyidi, F. Vaz, The influence of annealing treatments on the properties of Ag:TiO_2 nanocomposite films prepared by magnetron sputtering, Applied Surface Science, 258 (2012) 4028-4034.

[90] Z. H. Zhang, H. J. Wu, Y. Yuan, Y. J. Fang, L. T. Jing, Development of a novel capillary array photocatalytic reactor and application for degradation of azo dye, Chemical Engineering Journal, 184 (2012) 9-15.

[91] W. K. Jo, H. J. Kang, Photocatalytic performance of cylindrical reactor inserted

with UV light-emitting-diodes for purification of low-level toxic volatile organic compounds, Applied Surface Science, 259 (2012) 657-663.

[92] K. Baransi, Y. Dubowski, I. Sabbah, Synergetic effect between photocatalytic degradation and adsorption processes on the removal of phenolic compounds from olive mill wastewater, Water Research, 46 (2012) 789-798.

[93] Y. Sagatelian, D. Sharabi, Y. Paz, Enhanced photodegradation of diisopropyl methyl phosphonate by the "Adsorb & Shuttle" approach, Journal of Photochemistry and Photobiology A: Chemistry, 174 (2005) 253-260.

[94] W. J. Weber Jr., J. C. Morris, Kinetics of adsorption on carbon from solution, Journal of the Sanitary Engineering Division ASCE, 89 (1963) 31-60.

[95] K. V. Kumar, K. Porkodi, F. Rocha, Langmuir-Hinshelwood kinetics – A theoretical study, Catalysis Communication, 9 (2008) 82-84.

[96] G. Zayani, L. Bousslmi, F. Mhenni, A. Ghrabi, Solar photocatalytic degradation of commercial textile azo dyes: Performance of pilot plant scale thin film fixed-bed reactor, Desalination, 246 (2009) 344-352.

[97] R. Nagaraja, N. Kottam, C. R. Girija, B. M. Nagabhushana, Photocatalytic degradation of Rhodamine B dye under UV/solar light using ZnO nanopowder synthesized by solution combustion route, Powder Technology, 215-216 (2012) 91-97.

[98] S. Merabet, A. Bouzaza, D. Wolbert, Photocatalytic degradation of indole in a circulating upflow reactor by UV/TiO$_2$ process – Influence of some operating parameters, Journal of Hazardous Materials, 166 (2009) 1244-1249.

[99] H. Y. Zhu, R. Jiang, Y. Q. Fu, Y. J. Guan, J. Yao, L. Xiao, G. M. Zeng, Effective photocatalytic decolorization of methyl orange utilizing TiO_2/ZnO/Chitosan nanocomposite films under simulated solar irradiation, Desalination, 286 (2012) 41-48.

[100] Y. R. Zhang, J. Wan, Y. Q. Ke, A novel approach of preparing TiO_2 films at low temperature and its application in photocatalytic degradation of methyl orange, Journal of Hazardous Materials, 177 (2010) 750-754.

[101] F. Ahmedchekkat, M. S. Medjram, M. Chiha, A. M. A. Al-bsoul, Sonophotocatalytic degradation of Rhodamine B using a novel reactor geometry: Effect of operating conditions, Chemical Engineering Journal, 178 (2011) 244-251.

[102] X. Qin, L. Q. Jing, G. H. Tian, Y. C. Qu, Y. J. Feng, Enhanced photocatalytic activity for degrading Rhodamine B solution of commercial Degussa P25 TiO_2 and its mechanisms, Journal of Hazardous Materials, 172 (2009) 1168-1174.

[103] S. Q. Zhang, L. Chen, H. B. Liu, W. Guo, Y. X. Yang, Y. H. Guo, M. X. Huo, Design of $H_3PW_{12}O_{40}$/TiO_2 and Ag/$H_3PW_{12}O_{40}$/TiO_2 film-coated optical fiber photoreactor for the degradation of aqueous rhodamine B and 4-nitrophenol under simulated sunlight irradiation, Chemical Engineering Journal, 200-202 (2012) 300-309.

Acknowledgement

I sincerely thank my advisor, Professor Zhenya Zhang, for his supervision, encouragement and substantial support during my study in the University of Tsukuba. I also wish to express my heartfelt appreciation to my co-supervisor, Professor Yingnan Yang, for her detailed guidance, support and friendship during my doctoral studies. Her professionalism and hardworking is an excellent example I can follow throughout my future career.

I would also like to express my great gratitude to my dissertation committee members, Professor Zhenya Zhang, Yingnan Yang, Motoo Utsumi and Zhongfang Lei, for their patient reading, numerous comments and invaluable suggestions to serve as the committee members.

I also thank Professor Norio Sugiura for his numerous discussion and helpful suggestions throughout my dissertation research.

Special gratitude is expressed to University of Tsukuba and China Agricultural University for providing me the opportunity to pursue my study in Japan as a PhD student, and China Scholarship Council (CSC) for offering me the scholarship to complete my research.

I would also like to thank Professor Weizhong Jiang in China Agricultural University for giving me great motivation, encouragement and valuable suggestions to pursue higher education and improve research capability at University of Tsukuba.

Many friends and fellow students deserve recognition for their direct and indirect contributions to this dissertation. I wish to express my appreciation to

Qinghong Wang, Hanying Zheng, Yingxin Zhao, Xin Wang, Chengjie Han, Maohui Zhang, Qi Zhu, Cang Yu, He Huang, Leilei He, and many others for their countless assistance during the three years of my doctoral study in University of Tsukuba.

Finally, I would like to express deep gratitude to my dear parents and my girl friend Xuefei Yan. This dissertation would not have been completed without their love, encourage and support.

Appendix

1. **Dawei Li,** Tao Zhou, Ling Chen, Weizhong Jiang, Fan Chen, Baoming Li, Yutaka Kitamura. Using porphyritic andesite as a new additive for improving hydrolysis and acidogenesis of solid organic wastes. *Bioresource Technology*, Volume 100, Pages 5594-5599, December 2009. **(IF, 4.980; 5-Year Impact Factor: 5.352)**.

2. **Dawei Li**, Yingxin Zhao, Qinghong Wang, Yingnan Yang, Zhenya Zhang. Enhanced biohydrogen production by accelerating the hydrolysis of macromolecular components of waste activated sludge using TiO_2 photocatalysis as a pretreatment. *Open Journal of Applied Sciences*, Volume 3, Pages 155-162, June 2013.

3. Jingwen Lu, **Dawei Li**, Ling Chen, Yutaka Kitamura, Weizhong Jiang, Baoming Li. Simutaneous pretreatment and acidogenesis of solid food wastes by a rotational drum fermentation system with methanogenic leachate recirculation and andesite porphyry addition. *Bioresource Technology*, Volume 138, Pages 101-108, June 2013. **(IF, 4.980; 5-Year Impact Factor: 5.352).**

4. Ling Chen, Baoming Li, **Dawei Li**, Jing Gan, Weizhong Jiang, Yutaka Kitamura. Ultrasound-assisted hydrolysis and acidogenesis of solid organic wastes in a rotational drum fermentation system. *Bioresource Technology*, Volume 99, Pages 8337-8343, November 2008. **(IF, 4.980; 5-Year Impact Factor: 5.352).**

5. Fan Cheng, Ming Li, **Dawei Li**, Ling Chen, Weizhong Jiang, Yutaka Kitamura, Baoming Li. Volatile organic acid adsorption and cation dissociation by

porphyritic andesite for enhancing hydrolysis and acidogenesis of solid food wastes. ***Bioresource Technology***, Volume 101, Pages 5076-5083, July 2010. **(IF, 4.980; 5-Year Impact Factor: 5.352).**

6. Qinghong Wang, Yingnan Yang, **Dawei Li**, Chuanping Feng, Zhenya Zhang. Treatment of ammonium-rich swine waste in modified porphyritic andesite fixed-bed anaerobic bioreactor. ***Bioresource Technology***, Volume 111, Pages 70-75, May 2012. **(IF, 4.980; 5-Year Impact Factor: 5.352).**

7. Qinghong Wang, Yingnan Yang, **Dawei Li**, Chuanping Feng, Zhenya Zhang. Evaluation of a Ca-modified porphyritic andesite for ammonium removal in the anaerobic digestion process. ***Environmental Technology***, Volume 34, Pages 687-693, March 2013. **(IF, 1.606).**

8. Xin Wang, Motoo Utsumi, Yingnan Yang, Kazuya Shimizu, **Dawei Li**, Zhenya Zhang, Norio Sugiura. Removal of microcystins (LR, YR, RR) by highly efficient photocatalyst Ag/Ag_3PO_4 under simulated solar light condition. ***Chemical Engineering Journal***, 2013. (Accepted) **(IF, 3.461; 5-Year Impact Factor: 3.681).**

9. Chunguang Liu, Yingnan Yang, Qinghong Wang, Mijung Kim, Qingrong Zhu, **Dawei Li**, Zhenya Zhang. Photocatalytic degradation of waste activated sludge using a bed photocatalytic reactor for improving biohydrogen production. ***Bioresource Technology***, Volume 125, Pages 30-36, December 2012. **(IF, 4.980; 5-Year Impact Factor: 5.352).**